CROSS SECTIONS OF NUCLEI
FOR 1.4 BEV NEUTRONS

by

DAVID ALLEN HILL
A.B., Princeton University
(1951)

SUBMITTED IN PARTIAL FULFILLMENT
OF THE REQUIREMENTS FOR THE
DEGREE OF DOCTOR OF
PHILOSOPHY

at the

MASSACHUSETTS INSTITUTE OF
TECHNOLOGY

June, 1954

Signature redacted

Signature of Author ....
Department of Physics, May 10, 1954

Signature redacted

Certified by ....
Thesis Supervisor

Signature redacted

Accepted by ....
Chairman, Departmental Committee
on Graduate Students

Cross Sections of Nuclei for 1.4 Bev Neutrons
David Allen Hill
Submitted to the Department of Physics on May 11, 1954 in
partial fulfillment of the requirements for the degree of
Doctor of Philosophy.

Abstract

A counter experiment has been performed at the Brookhaven
Cosmotron to measure the absorption and total cross section of
several nuclei for neutrons in the Bev range. The neutrons are
produced by bombarding a Be target with 2.2 Bev protons. The
neutron detector is a proton recoil device which requires the
incident particle to pass an anticoincidence counter and produce
in an aluminum radiator a charged particle that will traverse a
four-fold scintillation counter telescope containing 6" of lead.

The angular distribution of neutrons from the target is
sharply peaked forward with a half width at half maximum of 6°.
The absolute flux of neutrons with energies greater than about
0.75 Bev is estimated from an emulsion exposure.

Using a narrow collimated beam the integral angular dis-
tribution of diffraction-scattered neutrons from C, Cu, and Pb is
measured by varying the detector geometry. The angular half-width
of the distribution indicates a mean effective neutron energy
of 1.4 $\pm$ 0.2 Bev, this value is nearly a linear average over
the effective spectrum. It is believed that contributions from
neutrons below about 1.0 Bev is small. The absolute detector
threshold is 0.4 Bev.

Using the narrow collimated neutron beam the total cross
sections σ_H and $\sigma_D - \sigma_H$ are measured by attenuation differences
in good geometry of CH_2-C and D_2O-H_2O respectively with the result:

$$\sigma_{tot} (H) = (42.4 \pm 1.8) \times 10^{-27} cm^2$$
$$\sigma_{tot} (D-H) = (42.2 \pm 1.8) \times 10^{-27} cm^2$$

The cross sections of eight elements from Be to U are measured
in good and poor geometry; the theoretical angular distribution
of Fernbach, Serber, and Taylor is used to extrapolate the measured
values to total and absorption cross sections respectively. An
important correction to the poor geometry cross section is necessary
because of the reduced detection efficiency for scattered particles.
The results are:

Total and Absorption Cross Sections
for Neutrons of Mean Energy 1.4 Bev

	σ_{tot}	σ_{abs}
Be	310	190
C	380	200
Al	700	410
Cu	1390	670
Sn	2200	1160
Pb	3210	1730
Bi	3280	1790
U	3640	1890

Cross sections are in
units of $10^{-27} cm^2$.

Experimental errors are
about 3% in σ_{tot},

5% in σ_{abs}.

The absorption cross sections are interpreted in terms of a uniform density nuclear model using an effective cross section of 43 mb for bound nucleons. The derived radii are well represented by $R = (-.05 + 1.28 A^{1/3})$ x 10^{-13}cm. The scattering cross sections of these eight elements are consistent with the single value $k_1 = (0.15 \pm 0.05)$ x 10^{13} cm^{-1} for the change in wave number within the nucleus.

The results can also be fitted with a gaussian-density nuclear model, i.e. $\rho = \rho_0 \, exp-\left(\frac{r}{a}\right)^2$ with a = $(0.32 + 0.62A^{1/3})$ x 10^{-13} cm.

A nuclear density distribution intermediate between uniform and gaussian will make the present results consistent with the recent electromagnetic radii.

Thesis Supervisor: Robert W. Williams
Title: Assistant Professor of Physics

Foreword

This experiment attempts a rather extensive program and from the beginning was conceived as a group project. The work of planning the experiment, setting up the equipment, and taking data was shared by Drs. T. Coor, W. F. Hornyak, L. W. Smith, G. A. Snow, and the author. The experimental work might be subdivided into four parts: (1) analysis of the forward neutron beam of the Cosmotron (2) the measurement of hydrogen and deuterium cross sections (3) the measurement of the integral angular distribution of diffraction scattering and (4) the measurement of good and poor geometry cross sections for several nuclei. The work of part (2) is more specifically the author's. It is thought best to report the work as a whole since the results of the entire program must be drawn upon in interpreting individual results.

The responsibility for assembling the data; calculating the results, corrections, and errors; and preparing this presentation has been primarily the author's; the help and encouragement given by the other members of the group is gratefully acknowledged. The method of interpreting the good and poor geometry cross sections in terms of the uniform-density optical model was suggested by Dr. G. A. Snow. The author performed the calculation and extended the method to the gaussian density model.

Table of Contents

List of Figures

List of Figures - continued

List of Tables

Notation

The notation used throughout is that of Fernbach, Serber, and Taylor (3). For convenience, it is collected here:

k wave number of the incident neutron

k_1 Increment in the wave number within the nucleus

K absorption constant in nuclear matter

R nuclear radius

σ_A nuclear absorption cross section. (In the sense of the optical model, σ_A includes not only true absorption but also inelastic scattering and scattering with exchange.)

σ_D diffraction scattering cross section

σ_T total nuclear cross section

$$\sigma_T = \sigma_A + \sigma_D$$

$\bar{\sigma}$ average cross section for bound nucleons

I Introduction

The measurement of nuclear cross sections for protons and neutrons in the energy range of 40 to 400 Mev has been an active subject in the past few years during which the high-energy machines at Berkeley, Chicago, Harwell have been in operation. The interest in this subject arises from the information which is gained about the nuclear radius and the gross features of nuclear structure since it was shown that nuclei exhibit a considerable transparency (1) for nucleons of this energy.

While the literature on neutron-nuclei cross sections above 40 Mev is extensive, the emphasis has been largely on transmission experiments in good geometry to measure total cross sections. In several cases, inelastic cross sections have been measured in bad geometry and, in a few cases, differential scattering experiments have been done. The observed total cross sections above 40 Mev can be roughly described as decreasing as 1/E until a plateau value is reached at about 200 Mev. The nuclear absorption cross sections are approximately independent of energy in this range and account for somewhat more than half the total cross section above 200 Mev. A partial list of previously reported total and absorption cross sections is given in Chapter V, Table 7. The relation of the results of the

present experiment to previous work is discussed in that chapter.

The current approach to the interpretation of nuclear cross sections at these energies begins with a drastically simplified nuclear model. For example, the analysis of Feshbach and Weisskopf (2) pictures the nucleus as a completely absorptive sphere. They have considerable success in explaining the trend of total and absorption cross sections in the energy region above 10 Mev by extracting results from this model with a partial wave analysis. However, the partial wave method becomes unwieldy at much higher energies: to describe the interaction of 1.4 Bev neutrons with the lead nucleus, partial waves up to order $\ell \sim 80$ must be carried. Fernbach, Serber, and Taylor (3) neatly avoid this inconvenience by making the classical approximation that at high energies the wave normals (or particle trajectories) are not distorted in passing through nuclear matter. The wave which traverses the nucleus suffers attenuation and advance in phase (for an attractive potential); the amplitude and phase distribution of the transmitted wave is readily calculated by ray tracing. Given this distribution, the absorption and diffraction cross sections are derived in terms of the nuclear radius, R, the absorption constant K, and the increment, k_1, in the propagation constant. The amplitude and phase distribution

- 2 -

of the transmitted wave near the nucleus sets the boundary value for the scattered wave; the angular distribution of the scattered wave is gotten by solving this well known boundary value problem for the wave equation. Fernbach, Serber, and Taylor have shown that this solution is equivalent to the partial wave analysis using a WKB method to calculate the phase shifts: comparisons with the exact partial wave solution for aluminum at 90 Mev have been made by Pasternack and Snyder (4). The classical approximation takes account of the transparency of nuclei for high energy nucleons but neglects the effect of refraction in nuclear matter and reflection at the nuclear surface. It is expected that this approach will become more valid with increasing energy.

The present experiment proposes to extend previous nuclear cross section measurements by using neutrons in the 1-2 Bev range; the purpose being to provide a further bit of information by which current theories may be tested and to explore the new features which may appear at these energies. The experiment is made possible by the intense beam of Bev neutrons generated in the Brookhaven Cosmotron by the impact of 2.2 Bev protons on a beryllium target. By using neutrons rather than protons for such measurements, one gains the obvious advantage that the nuclear interaction is not masked by Coulomb effects. The presence of Coulomb forces influences the result in two ways; first,

through the direct interference of Coulomb and nuclear amplitudes for small angle scattering and, secondly, through the effect of multiple Coulomb scattering. A concurrent experiment done by Chen (5) on the interaction of 870 Mev protons with nuclei points up the difficulty of interpreting the proton results. On the other hand, the experimental difficulties are multiplied in a neutron measurement by the small efficiency and poor energy resolution of neutron detectors. In the present experiment, it has been necessary to accept neutrons over the broad energy range of roughly 1 to 2.2 Bev in order to achieve a usable counting rate. The resulting average cross sections are significant if the cross section is only a slowly varying function of energy over this range; this is thought to be the case.

The experiment is specifically designed to determine:

1. The neutron-proton and neutron-neutron total cross sections by measuring attenuation differences of $C-CH_2$ and D_2O-H_2O in good geometry.

2. The total and absorption cross sections of several nuclei by attenuation measurements in good and bad geometry.

3. The integral angular distribution of diffraction scattering. This is done as a rough test of the theoretical prediction and yields a value for the mean effective neutron energy.

- 4 -

In the following presentation, Chapter II describes the experimental apparatus and the preliminary work that was done to analyze the neutron beam. The experimental procedure and the reduction of data are explained in Chapter III. In Chapter IV the experimental cross sections are analyzed in terms of a uniform density and a gaussian density nuclear model. Chapter V relates the results to previous work and indicates some conclusions.

The principal results might be briefly summarized here:

1. For a neutron spectrum of mean effective energy 1.4 Bev, the elementary total cross section, σ_{N-P}, is found to be 42.4 ± 1.8 mb. If the simple addition $\sigma_{ND} = \sigma_{N-P} + \sigma_{N-N}$ is valid, the total n – n and n – p cross sections are equal at this energy and considerably larger than their value in the 300 Mev region.

2. The absorption cross sections of Be, C, Al, Cu, Sn, Pb, Bi, and U for 1.4 Bev neutrons can be consistently interpreted in terms of a uniform-density nuclear model of radius, $R = (-.05 + 1.28\ A^{1/3})\ 10^{-13}$ cm. For the heavy elements, the absorption cross section determines the nuclear radius quite directly since the correction for nuclear transparency is small.

3. The diffraction scattering cross section of these elements for 1.4 Bev neutrons represents about 47% of the total for the heavy elements; this fraction is reduced to about 42% for the light elements.

II Experimental Apparatus and Analysis of the Beam

Cosmotron Characteristics

Since the characteristics of the Brookhaven Cosmotron (6) create some unique experimental problems and opportunities perhaps it is well to briefly describe the machine. The Cosmotron is a proton synchrotron of impressive proportions; the magnet is constructed in four quadrants separated by straight sections to form a racetrack of 30 foot radius. A pulsed magnetic field of 14 kilogauss maximum is provided throughout a stainless steel vacuum chamber 36" in radial dimension and 7" high. Radio frequency drive is magnetically coupled to the proton beam in one of the straight sections. Protons are injected into the machine from a 4 Mev Van de Graaff machine and accelerated for 950 milliseconds during which the driving frequency is swept from about 0.4 to 4 Mc. as the magnetic field increases. At the end of the acceleration cycle, the driving voltage is gradually reduced to collapse the proton orbit bringing approximately 10^{10} protons into a beryllium target within an interval of 30 milliseconds. The acceleration cycle is repeated every 5 seconds. During the bombardment a copious beam of energetic neutrons from charge exchange and inelastic interactions is projected in the forward direction.

Neutron Detector

In order to use this beam for nuclear measurements,

- 7 -

one would desire a neutron detector having:

1. an energy threshold in the 1-2 Bev range

2. a constant or, at least, a known detector efficiency as a function of neutron energy

3. a reasonable efficiency for neutrons and, at the same time, insensitivity to gamma rays and charged particles.

4. a resolving time of the order of 10^{-8} seconds so that coincidence technique can be used.

Experimenters at lower energies have made useful neutron detectors employing the activation of carbon (the C^{12} (n, 2n)C^{11} reaction) which has a threshold of 20 Mev, the neutron-induced fission of bismuth detected with an ion chamber (a threshold of 50 Mev), and proton-recoil detectors in which an energy threshold is set either by a minimum range required of the proton or by a minimum velocity required in a Cerenkov detector. But, in extending the threshold of the proton recoil-range type of detector to the Bev region, the efficiency drops rapidly because of nuclear absorption of the recoil particles; for example, a 1 Bev proton has a range in lead of greater than 3 absorption lengths. One might hope to avoid this by observing the less energetic recoils at large angles but the cross section for such events presumably falls off rapidly.

The difficulty in extending the threshold of the proton-recoil-Cerenkov type of detector arises from the

fact that the velocity is not a sensitive function of
energy for protons in this energy range (for protons of
500 Mev, β = .74; of 1 Bev, β = .87; of 2 Bev, β = .94).
The possibility of meson production further complicates
the problem.

Another possibility that suggests itself is the
use of magnetic analysis of the recoil protons either by
the usual momentum separation in a magnetic field or by
means of a momentum dependent focussing arrangement. For
protons in the Bev range cumbersome magnets and large
deflection distances are required; the resulting small
solid angle for collection of recoil protons precludes a
reasonable efficiency.

In spite of the obvious limitations, we have
adopted essentially a proton recoil-range detector using a
6" Pb absorber as a reasonable compromise between energy
threshold and efficiency. Figure 1 shows the disposition
used. Neutrons are detected by requiring them to traverse
an anti-coincidence counter A and produce in an aluminum
radiator charged particles which penetrate a 4-fold
scintillation counter telescope containing 6" of Pb. The
threshold for this process is 400 Mev if the charged particle
is a proton produced in an elastic charge exchange process
in the radiator. A secondary charged meson of 240 Mev
produced in the radiator can also penetrate 6" of Pb but

- 9 -

$C_1 - C_4$ PLASTIC SCINTILLATORS 2 1/2" DIA. 1/2" THICK
A PLASTIC SCINTILLATOR 4" DIA. 1/2" THICK

A

ALUMINUM
RADIATOR

C_1

C_2

6"

C_3

C_4

NEUTRON
BEAM

2"

LEAD ABSORBER

IP2I

16 1/2"
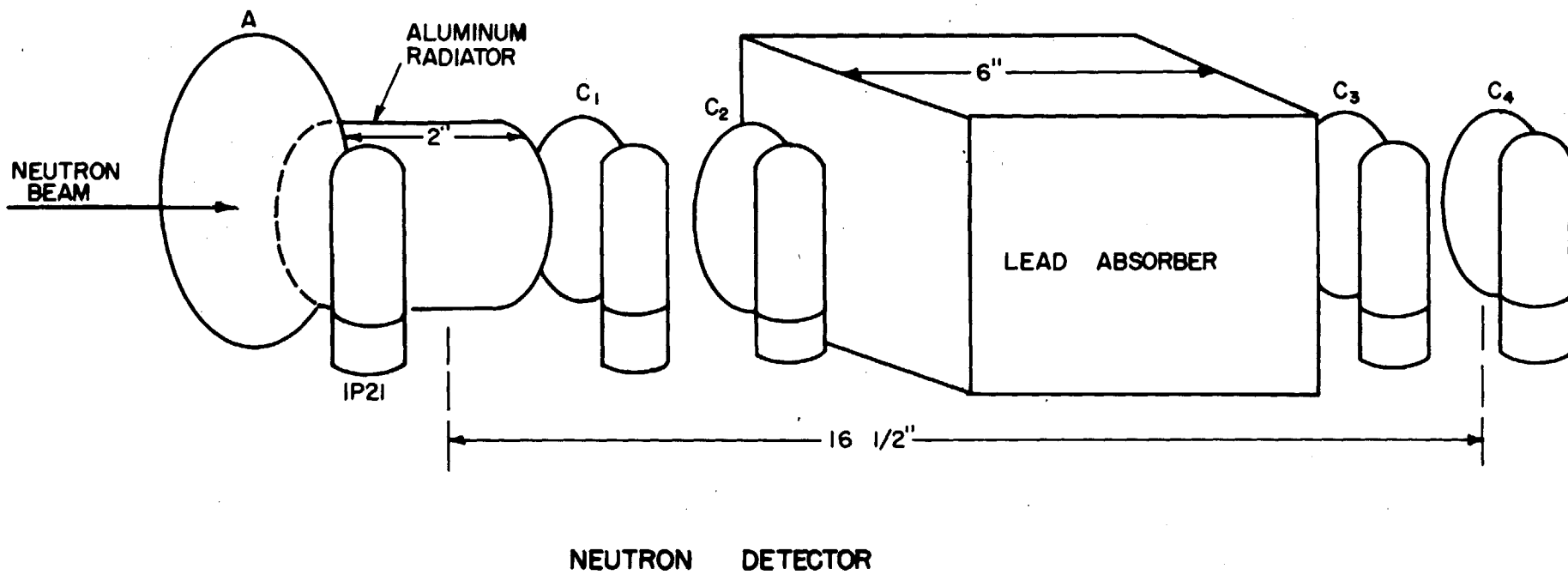
Figure 1

NEUTRON DETECTOR

this requires an incident neutron of at least 540 Mev.
For neutron energies above threshold, this detector should
favor the higher energies since it requires a charged
secondary within a narrow cone (4.3° half angle) in the
forward direction.

The plastic scintillators are compression molded
of polystyrene activated with terphenyl and a trace of
diphenylhexatriene. Each scintillator is machined and
polished to be mounted directly on a 1P21 photomultiplier
tube with silicone fluid (Dow-Corning 200) providing good
optical contact. The crystals are covered with aluminum
foil and are held in place with a thin brass strap. The
whole assembly is then thoroughly wrapped with black plastic
tape.

The electronic circuitry is of standard design,
the general arrangement is shown in the block diagram of
Figure 2. The photomultiplier tubes are selected 1P21's
which operate without breakdown at an anode potential of
1600 - 1800 volts. The output signal is limited to about
2 volts with a biased crystal diode to prevent overloading
and led through 100 feet of cable to a wide band dis-
tributed amplifier (Hewlett-Packard Model 460 B). The four-
fold coincidence signal with anticoincidence from A is
formed in a circuit of the type described by Garwin (7);
it is then amplified and enters a fast discriminator

DETECTOR   CIRCUIT

A ◯ ──── [DIODE LIMITER] ──────── [DISTRIBUTED AMPLIFIER] ───── [COINCIDENCE C_1-C_4 WITH ANTI-COINCIDENCE A]

C_1 ◯ ──── [　　] ──────── [　　]

C_2 ◯ ──── [　　] ──────── [　　]

C_3 ◯ ──── [　　] ──────── [　　]

C_4 ◯ ──── [　　] ──────── [　　]

[FAST AMPLIFIER AND EFP 60 DISCRIMINATOR] ←── GATE

[FAST SCALE OF 8]

[SLOW SCALER AND REGISTER]

MONITOR   CIRCUIT

◯ ──────────────── [DISTRIBUTED AMPLIFIER] ───── [3-FOLD COINCIDENCE]

◯ ──────────────── [　　]

◯ ──────────────── [　　]

[FAST AMPLIFIER AND EFP 60 DISCRIMINATOR] ←── GATE

[FAST SCALE OF 8]
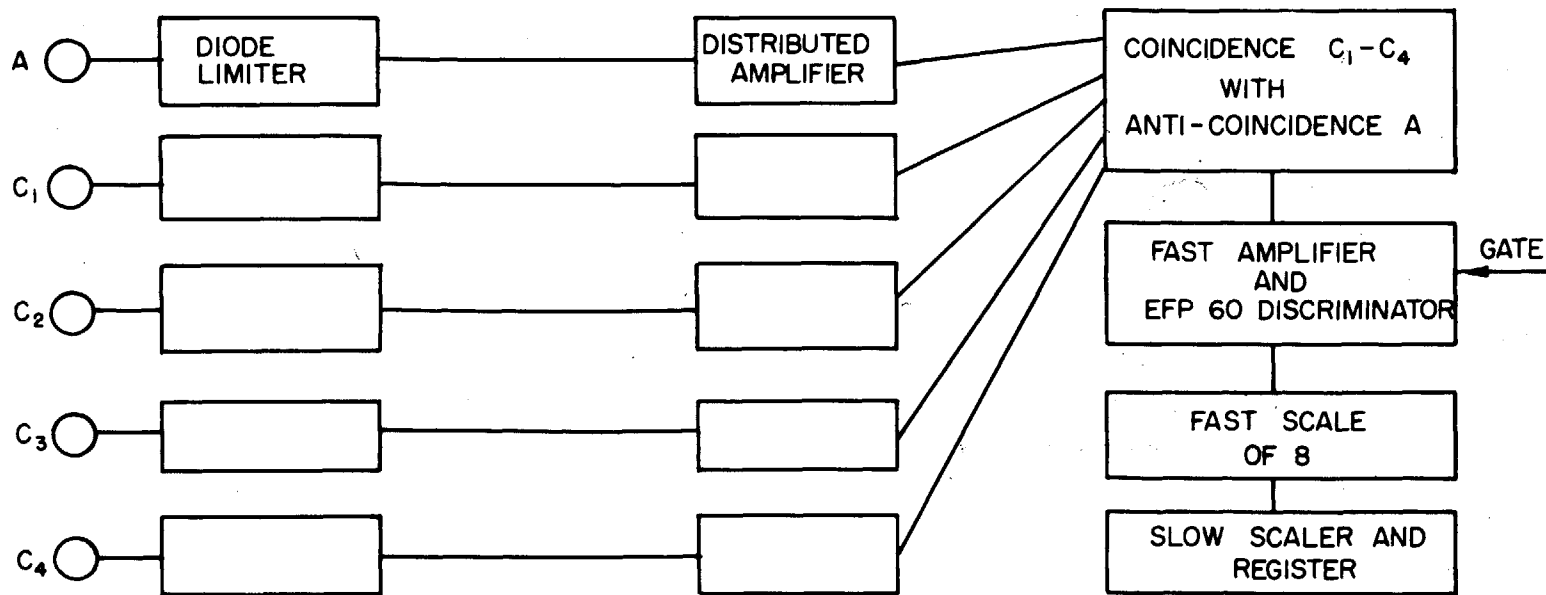
[SLOW SCALER AND REGISTER]
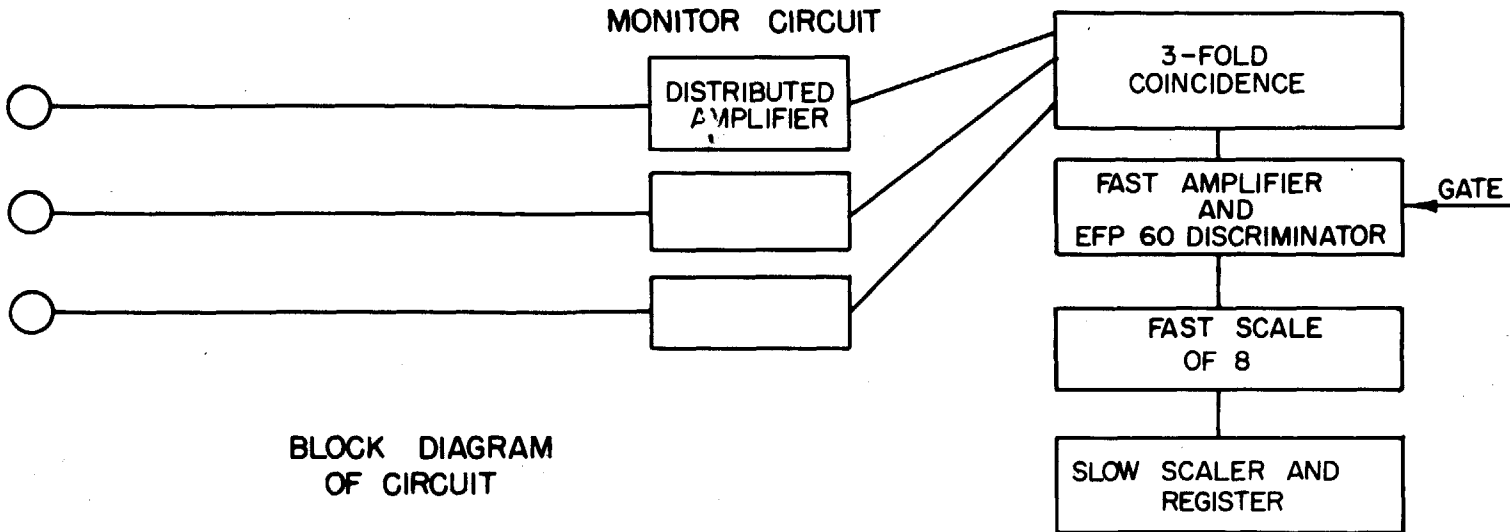
BLOCK   DIAGRAM
OF CIRCUIT

Figure 2

circuit using an EFP 60 secondary emission tube. The output pulses drive a fast scale of eight followed by a one microsecond scale of sixty four and register. The integral bias curve (Figure 3) obtained with this circuit shows a very satisfactory plateau for four-fold coincidences and an anti-coincidence counter efficiency of greater than 0.99. The circuit is gated on only for a short interval at 920 milliseconds after beam injection to prevent spurious counts due to "spillout" during the acceleration cycle.

The measured resolving time of the coincidence circuit is about 8×10^{-9} seconds (half width at half maximum response) and is probably determined by the decay time of the scintillator; improvement of this by pulse clipping has not been necessary. The amplifier and discriminator following the coincidence circuit have a measured recovery time of 0.8×10^{-7} seconds; the counting speed is limited by the scale of eight which has a recovery time of 2×10^{-7} seconds. With typical beam intensities, we obtain 10 to 20 counts in a 30 millisecond interval. The expected counting losses based on this average rate are negligible; however, the peak counting rates in this interval may be many times larger due to "bunching" of the internal proton beam. Occasionally bunching is observed corresponding to the 1 kc. synchrotron oscillations; whether this also occurs with the higher frequency of betatron oscillations is not known.

COINCIDENCE CIRCUIT BIAS CURVE

4 FOLD RATE C_1 C_2 C_3 C_4

A

C_1 C_2 C_3 C_4

ANTI-COINCIDENCE RATE
C_1 C_2 C_3 C_4 - A

COUNTING RATE RELATIVE TO MONITOR

DISCRIMINATOR BIAS (VOLTS)
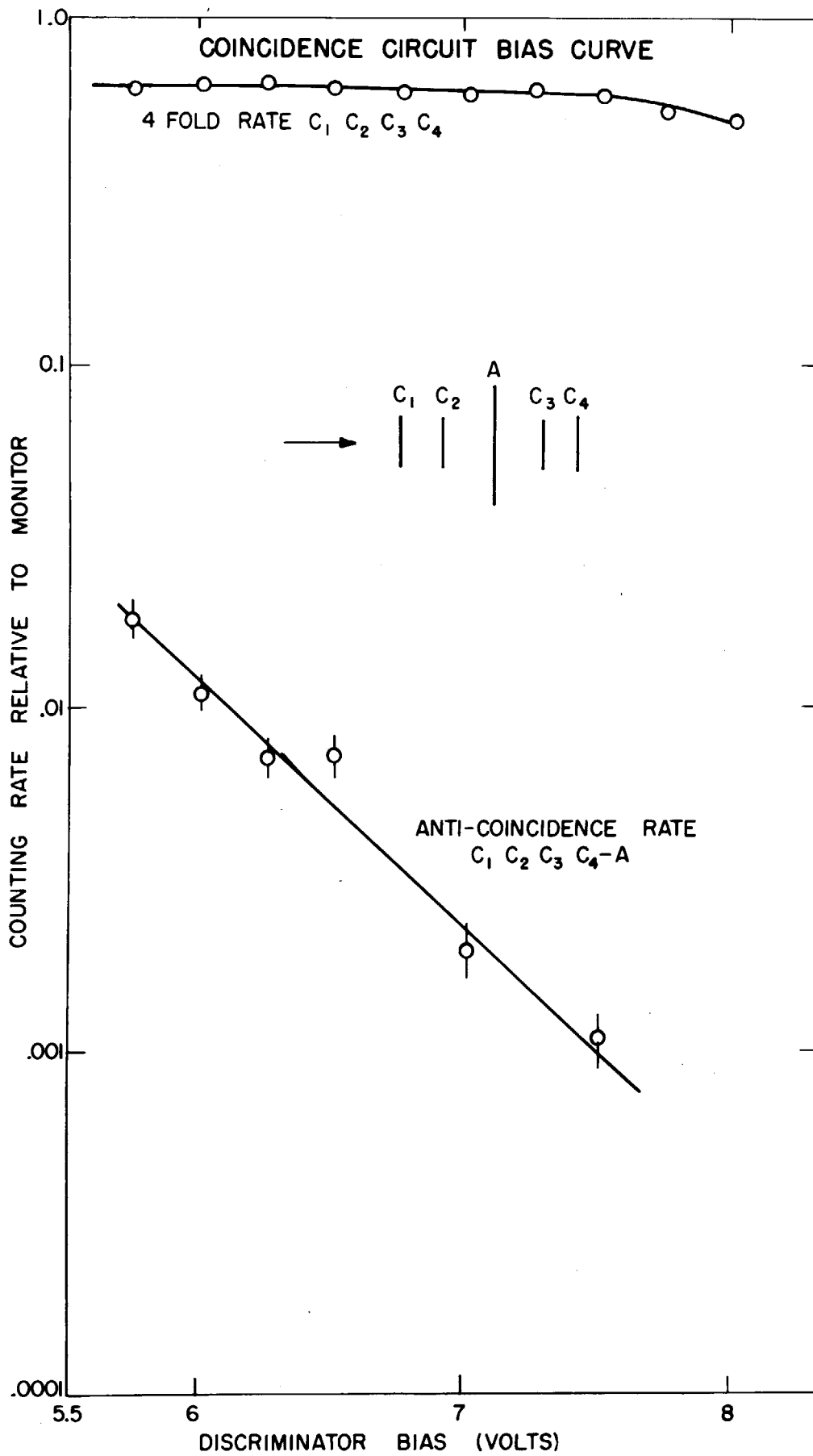
Figure 3

A monitor of the beam intensity is provided by a three fold counter telescope placed outside the shield in a beam which emerges at 3° to the forward direction. The telescope contains $1\frac{1}{2}$" of lead and is placed behind a 10" lucite radiator. The counting rate is roughly 200 per pulse and is attributed mainly to neutron conversion in the lucite since the counting rate with the lucite removed is several times smaller. The construction and circuitry for the monitor is very similar to that of the detector except that it does not have an anti-coincidence counter.

An estimate of the energy dependence of detection efficiency can be made from the excitation function shown in Figure 4. This curve is the ratio of the detector counting rate to the proton beam current striking the Cosmotron target as a function of the proton energy. (The proton beam current is monitored by measuring the voltage induced on a pair of pick-up electrodes through which the beam passes.) This steeply rising function of energy therefore represents the product of two probabilities: first, the probability that a proton striking the target will produce an energetic neutron in the forward direction either by charge exchange or by an inelastic collision and, secondly, the probability that an energetic neutron striking the aluminum radiator will produce an energetic charged secondary in the forward direction again either by an elastic or inelastic process. Because these two events

- 12 -
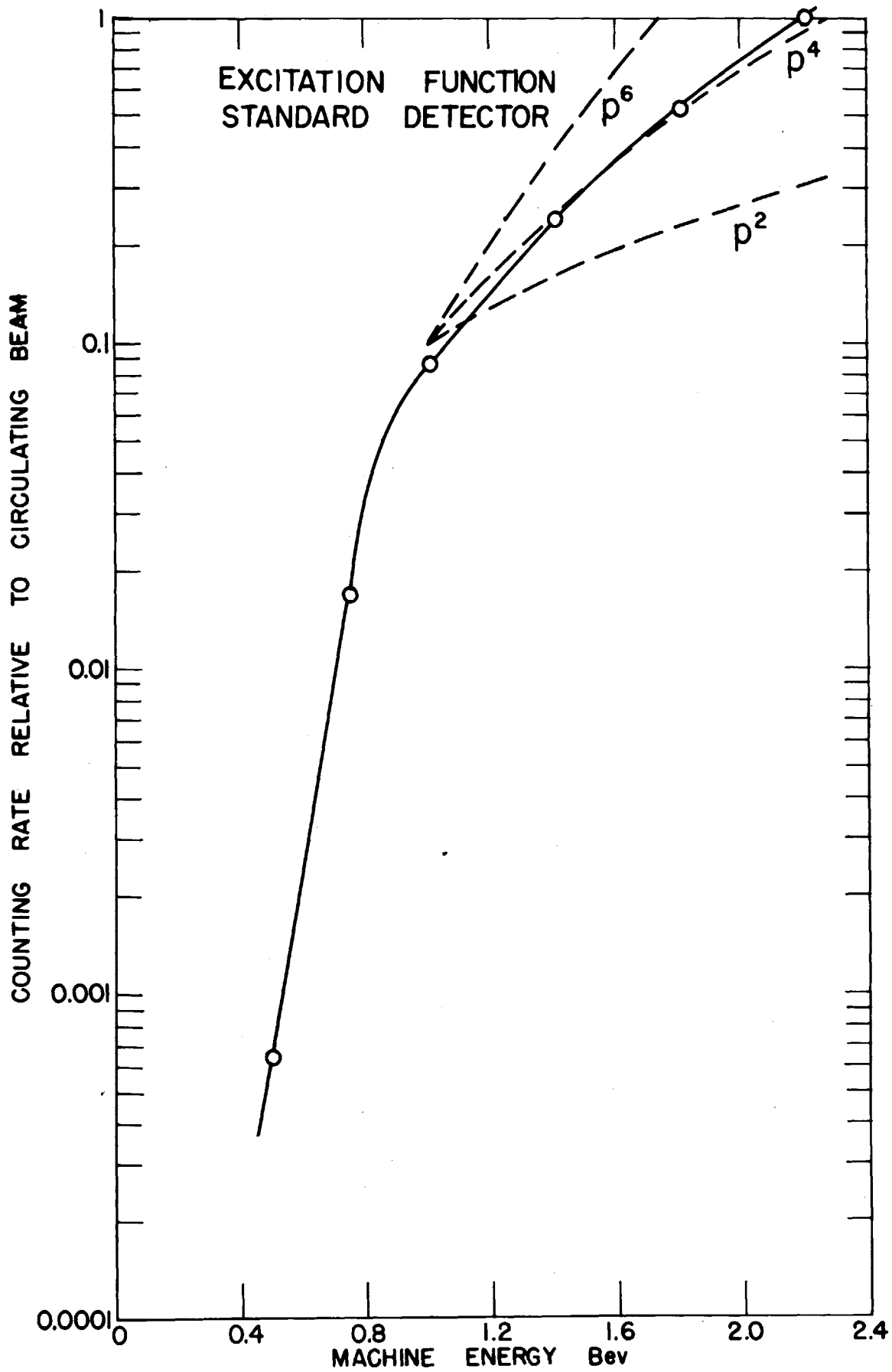
Figure 4

are similar, this function which shows a p^4 dependence between 1 and 2 Bev should represent roughly the square of the detector sensitivity.

Neutron Flux and Angular Distribution

An estimate of the neutron flux was obtained by exposing Ilford G-5 nuclear emulsions in the beam; the plates were then area-scanned for many-pronged events which typify the interaction of neutrons with energies above 0.5 - 1 Bev. Figure 5 displays the prong number distribution. Taking the number of stars with $N_4 \geq 8$ (an average energy release of $\sim$ 550 Mev among the slow secondaries) and the mean free path of 190 cm. for the production of stars with $N_4 \geq 9$ by 2.2 Bev protons (8), we calculate the flux 50 ft. forward of the target to be about 10^3 neutrons above .5 to 1 Bev per cm^2 per pulse. A comparison of this flux with the observed counting rate of the detector implies a detection efficiency of about 0.1%.

The angular distribution of energetic neutrons produced in the beryllium target was measured by moving the detector to the various available ports in the shielding which view the target. Figure 6 shows the results obtained at two proton energies after correcting the observed counting rates for the varying thickness of obstruction in the neutron path (at most 28% correction)

- 13 -

Figure 5

PRONG NUMBER DISTRIBUTION
FOR EMULSION EXPOSED
TO 0° NEUTRON BEAM

N_h: NUMBER OF GREY PLUS BLACK
PRONGS (SOME MINIMUM PRONGS
INCLUDED)

NUMBER OF STARS

N_h

ANGULAR DISTRIBUTION OF ENERGETIC
NEUTRONS FROM BERYLLIUM
TARGET

MACHINE ENERGY
2.2 BEV

MACHINE ENERGY
1.0 BEV

RELATIVE NUMBER PER UNIT SOLID ANGLE
(NORMALIZED TO CIRCULATING BEAM)

ANGLE FROM FORWARD DIRECTION
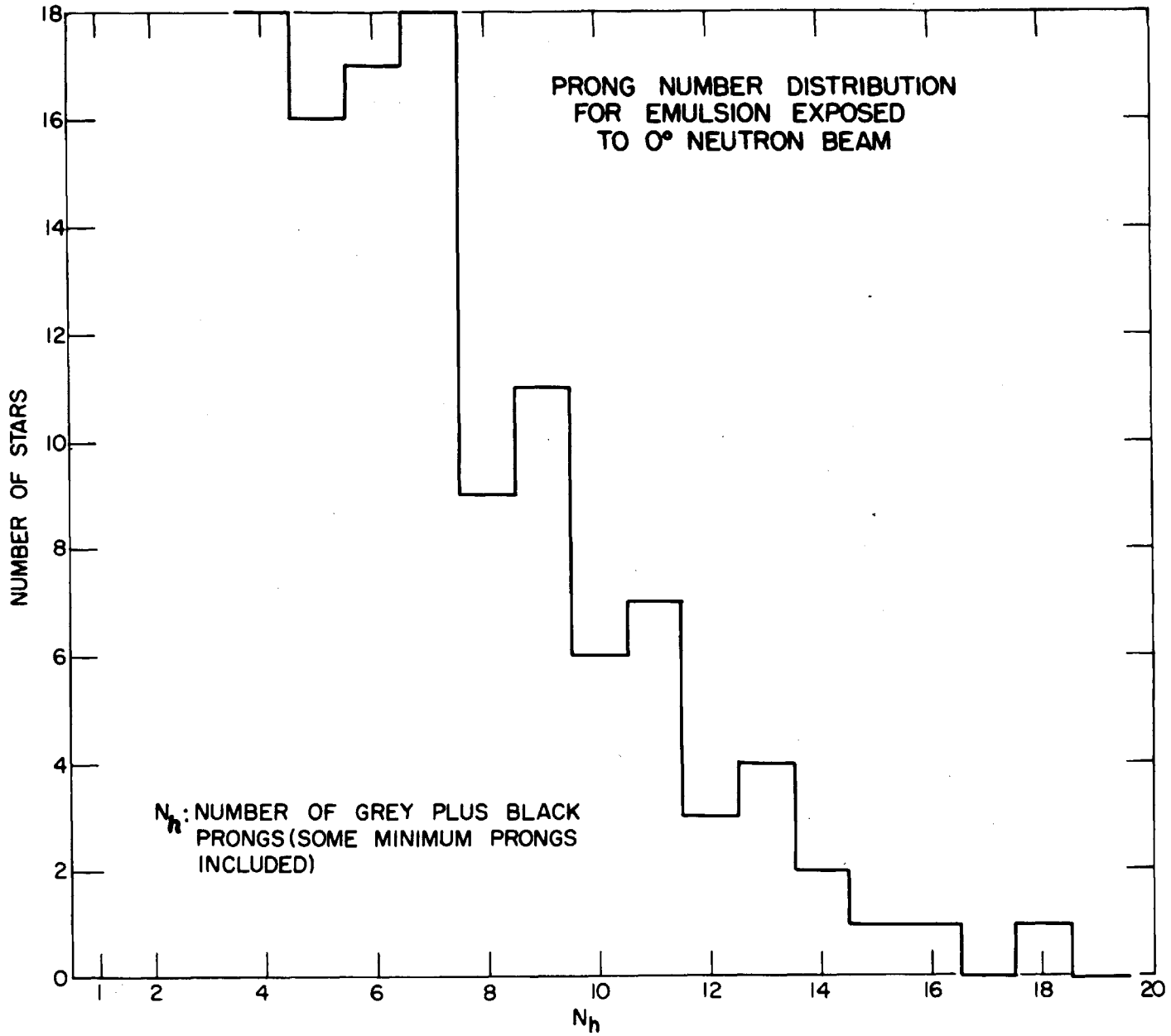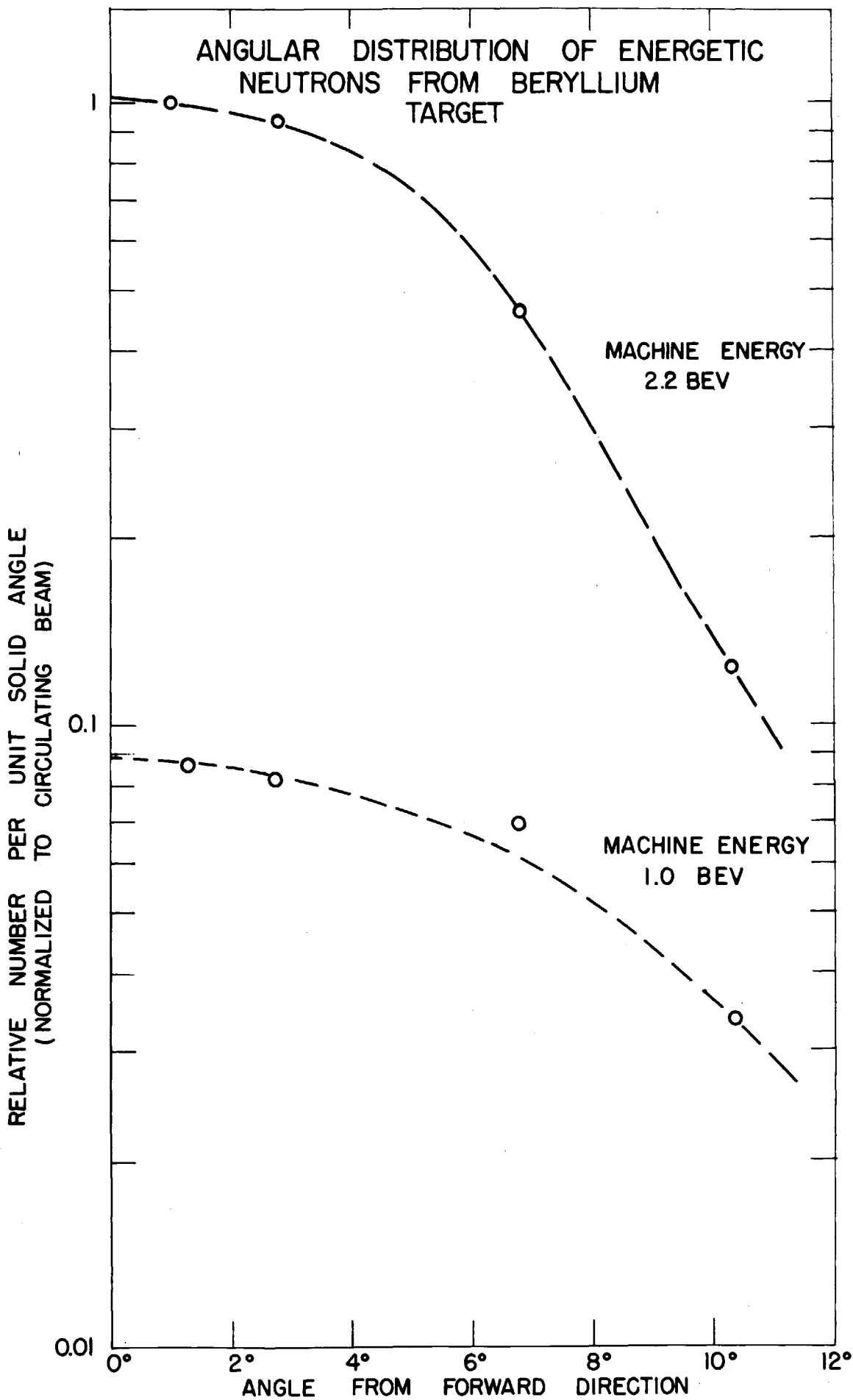
Figure 6

and the slightly different distances from the target to
the detector (at most 9% correction). The distribution is
strongly peaked in the forward direction having a half
width at half maximum of 6.5°; the distribution is similar
to that observed at Berkeley (9) with 340 Mev protons on a
beryllium target except that the angular width is reduced
by a factor of 3.5, the ratio of the incident proton momenta.

Production of Penetrating Charged Secondaries by Neutrons

For comparison, the angular distribution of
penetrating charged secondaries produced by neutrons in
beryllium, aluminum, and lead was measured with the arrange-
ment shown in Figure 7. The difference in counting rate
with the sample in and out was measured for several angles
up to 20°. This method would be in error if an appreciable
fraction of the incoming neutrons interact not in the sample
but in the 6" Pb absorber giving rise to charged particles
forward to trip counters 3 and 4 and charged particles back-
ward to trip counters 1 and 2. This effect was estimated
by putting the four fold telescope in the beam (setting ● = 0)
and moving counters 1 and 2 out of the beam so that a
single particle going forward from the converter cannot
traverse 1, 2, 3, and 4 but a single backward-going particle
from the lead can traverse 1 and 2. The contribution from
events of this type is at most 6% of the observed counting
rate. Figure 8 presents the observed angular distributions

- 14 -

NEUTRON BEAM

A

Be, Al OR Pb SAMPLES AS CONVERTER

C_1

C_2

6" LEAD

C_3

C_4

θ
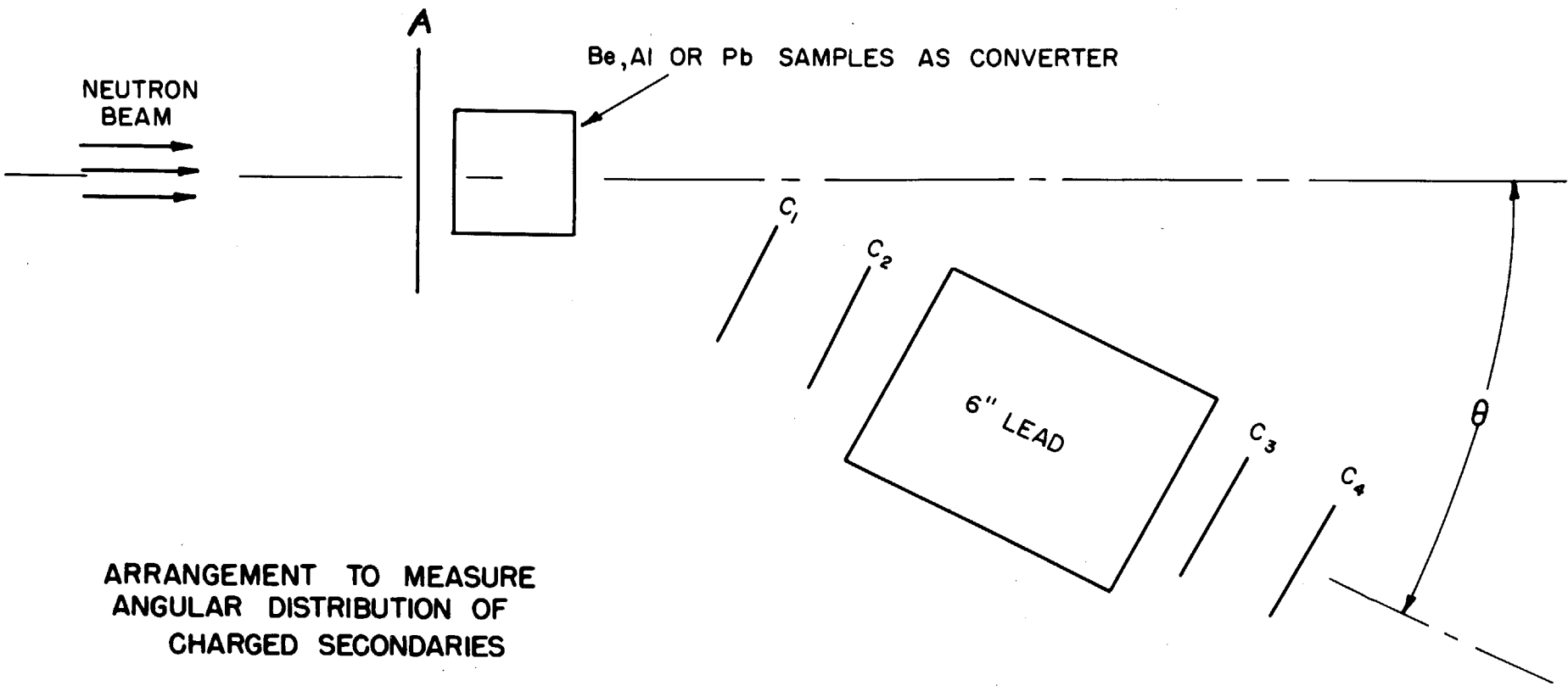
ARRANGEMENT TO MEASURE
ANGULAR DISTRIBUTION OF
CHARGED SECONDARIES

Figure 7

Figure 8

ANGULAR   DISTRIBUTION   OF   PENETRATING
CHARGED   SECONDARIES

x BERYLLIUM
o ALUMINUM
● LEAD
(ALL   NORMALIZED   TO
1.0   AT   0°)

RELATIVE   YIELD
PER   NUCLEUS
Be   .29
Al   .64
Pb   1.00

RELATIVE   NUMBER   PER   UNIT   SOLID   ANGLE
AVERAGED   OVER $\theta \pm 4.2°$

ANGLE   FROM   FORWARD   DIRECTION
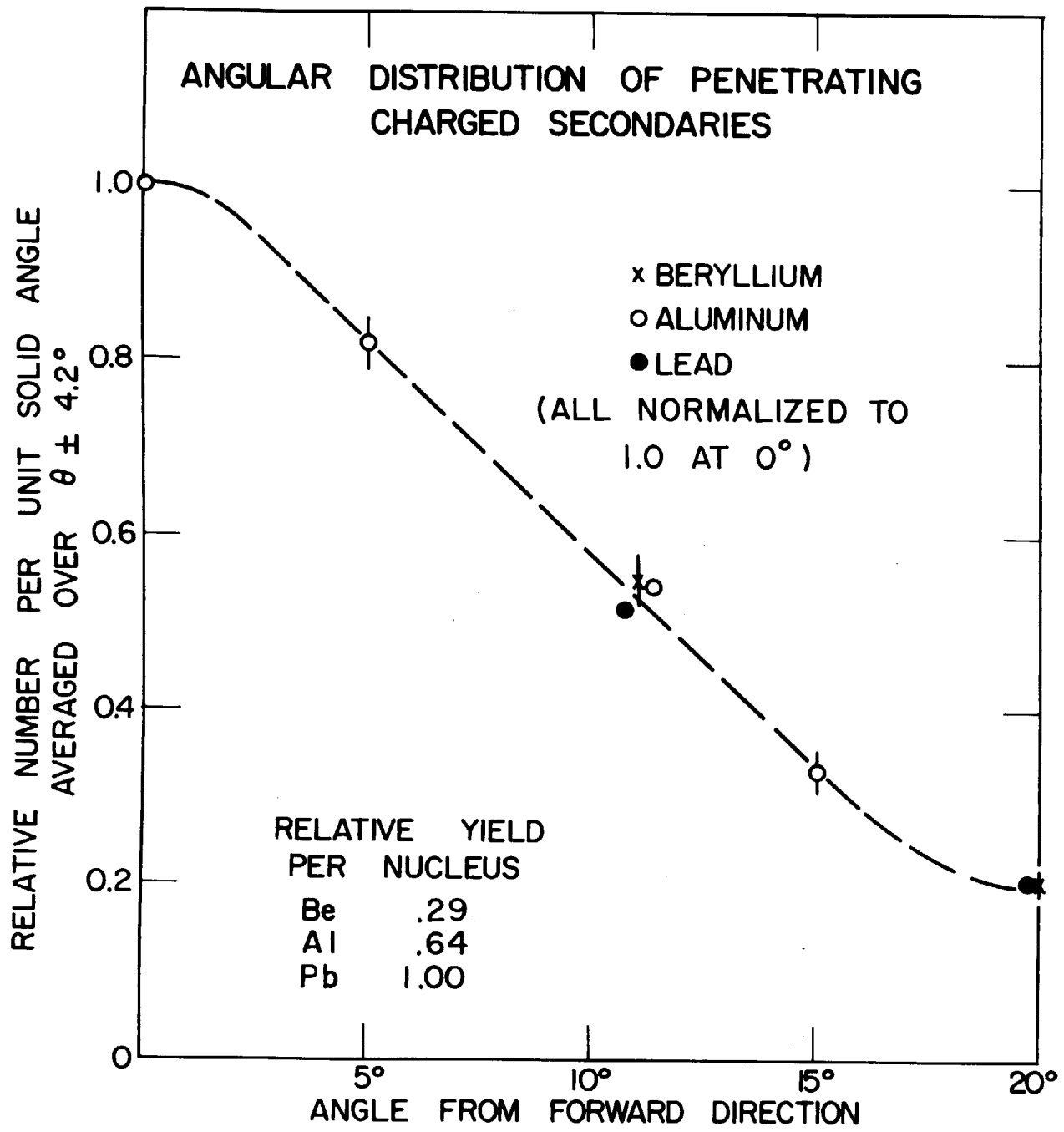
from beryllium, aluminum and lead. The angular resolution as determined by the half angle subtended by the last counter, C_4, at the converter is 4.2°. The distribution is strongly peaked forward and sensibly the same for these three elements. The relative yield per nucleus varies approximately as $A^{1/3}$ which suggests that mainly the nucleons around the perimeter of the nucleus contribute to this process, the central region being opaque.

Collimation of the Neutron Beam

In order to do transmission experiments the forward neutron beam is collimated by a 1" hole extending through 8 ft. of shielding concrete and 2 ft. of lead. The effectiveness of collimation can be seen in Figure 9 which shows the detector counting rate versus lateral displacement at a distance of 12' from the collimator exit. The measured dependence agrees with that expected from the overlap of a 1" diameter beam with a $2\frac{1}{2}$" diameter detector. With the detector aligned in the beam, the counting rate decreases by $(3.5 \pm 2)\%$ as the detector is moved from 3 feet to 12 feet from the collimator exit.
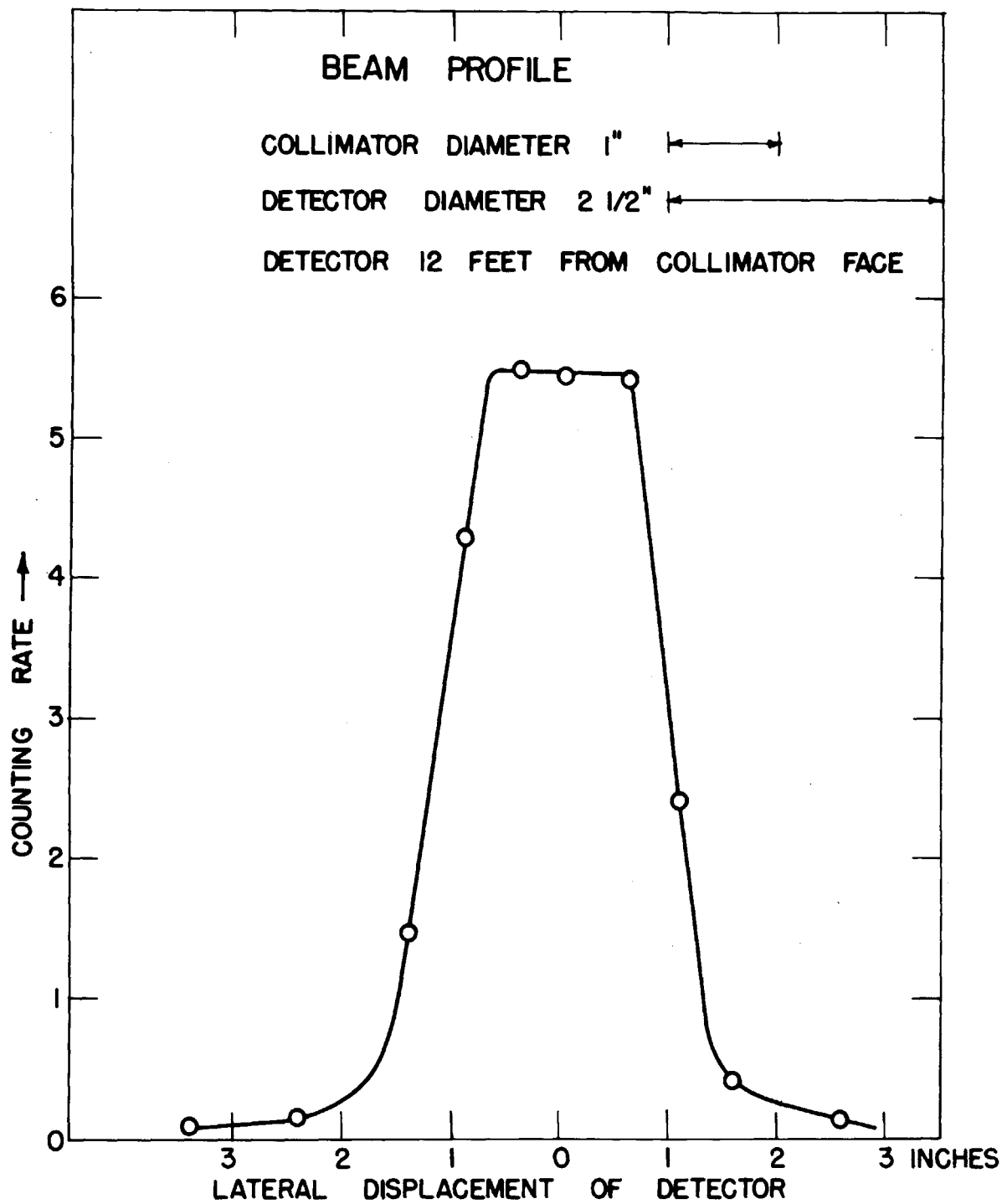
Figure 9

III Experimental Procedure and Results

Hydrogen and Deuteron Total Cross Sections

Using the 2" diameter collimated neutron beam described in the last section, the total n-p cross section was determined by measuring the attenuation in good geometry of polyethylene $(CH_2)_n$ and carbon. The samples used were of high purity and were chosen to contain the same thickness of carbon in grams per cm^2.

The difference $\sigma_D - \sigma_H$ was measured in the same way with samples of heavy water (D_2O) and ordinary water contained in thin-walled brass cylinders of equal length. Figure 10 and 11 show the disposition of scatterer and detector. The half angle θ subtended by the detector at the scatterer was normally about 0.7°; the divergence of the incident beam is of the order of 0.2°. Data is collected by alternating the samples after about 5,000 counts are recorded in the detector. The beam monitor is run concurrently and, in all cases, only the ratio of detector to monitor counts is used. One day's run comprises about 100,000 counts taken in this way. Table 1 displays the results of a typical run of 8 measurements on each sample.

The experimental arrangement was varied in the second n-p run by doubling the thickness of carbon and polyethylene used. In the third n-p run, the collimated beam was reduced to 1" diameter. The geometry was varied

PLAN VIEW NE QUADRANT OF COSMOTRON

MAGNET

PROTON ORBIT

TARGET

LEAD FILTER

DETECTOR

SCATTERER

MONITOR

SHIELD

| 0 | 10 | 20 |

SCALE IN FEET
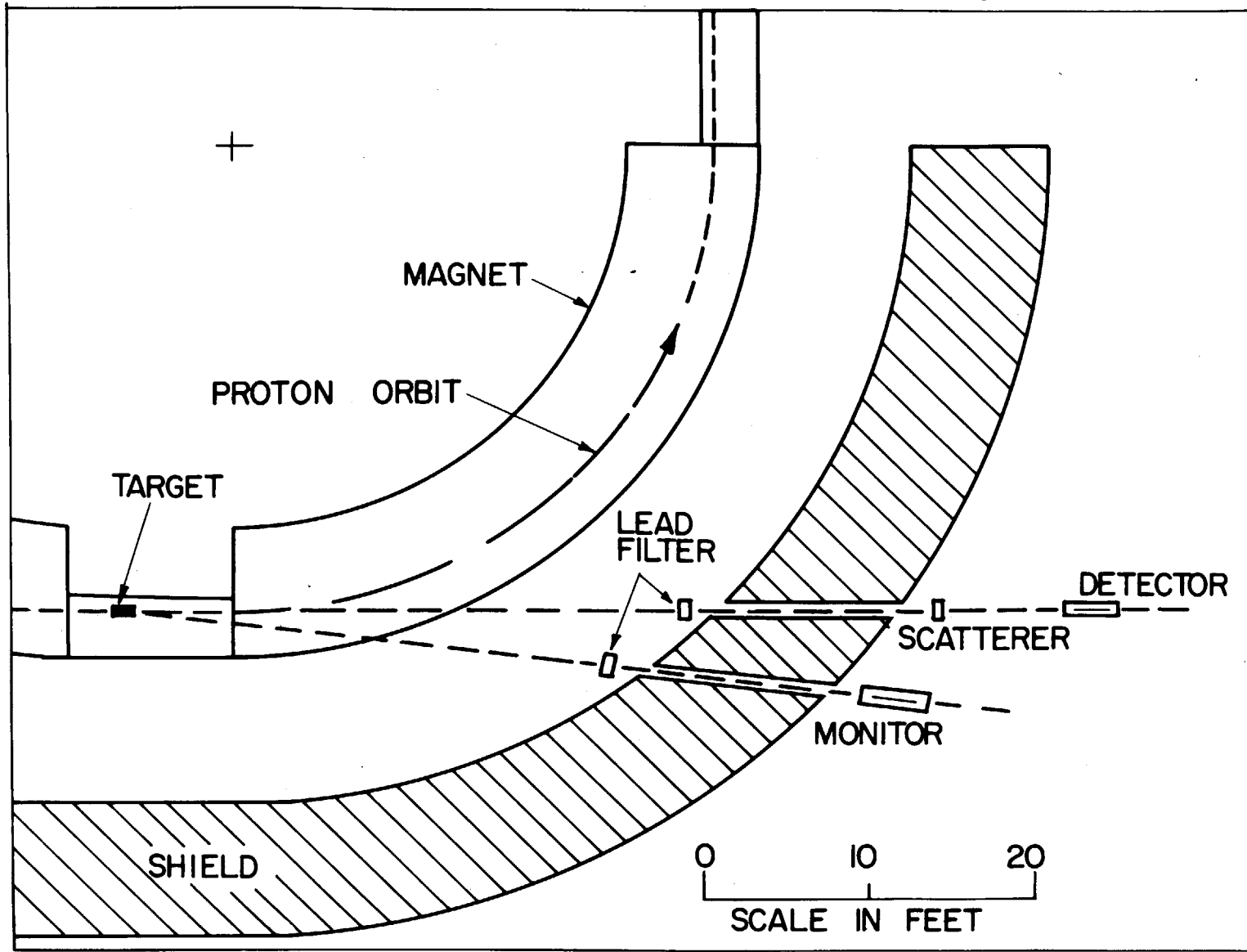
Figure 10

EXPERIMENTAL ARRANGEMENT FOR TRANSMISSION MEASUREMENTS

SHIELD

COLLIMATOR
I OR 2"DIA.

SCATTERER

θ

DETECTOR

ℓ

50' TO TARGET
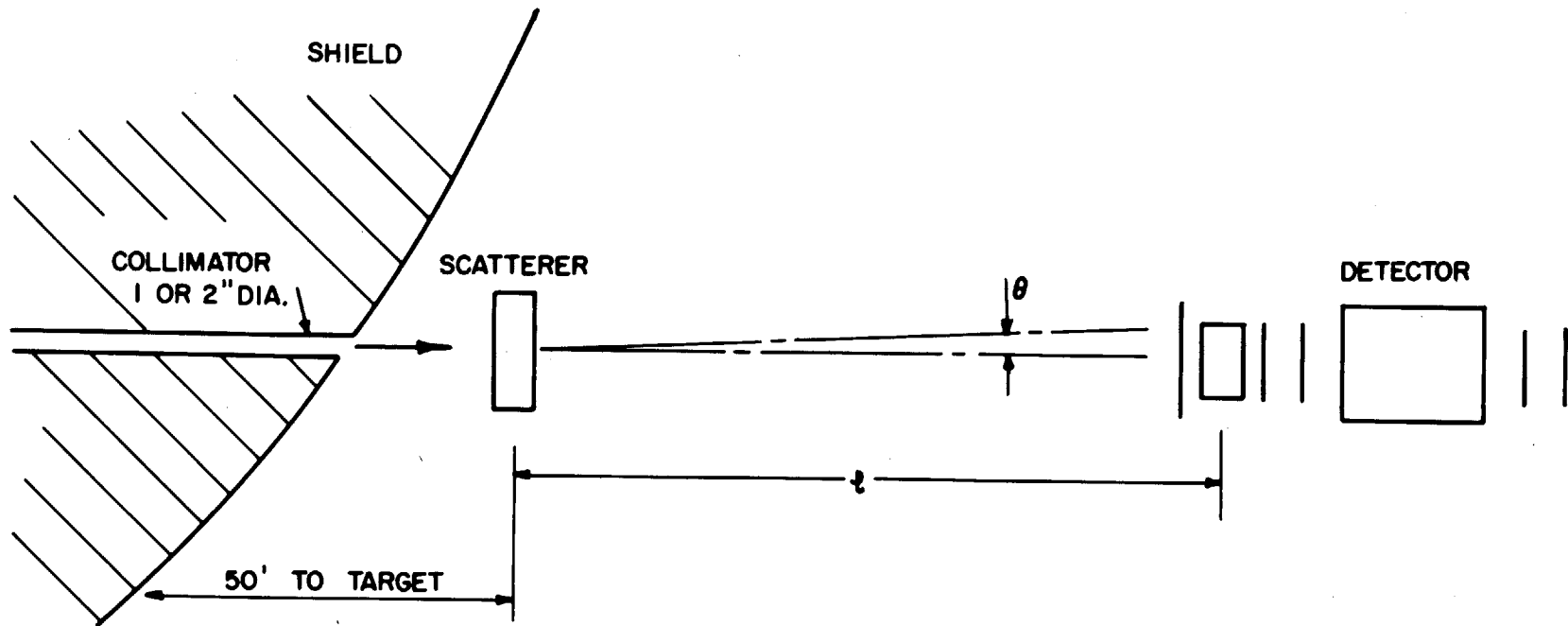
Figure 11

Table 1

Data from Typical Run of N – P Experiment

Scatterer	Monitor Counts (Units of 8)	Detector Counts (Units of 8)	Ratio $\frac{Det}{Mon}$
Out	1394	352	.2525
C	4234	646	.1526
CH₂	4692	644	.1373
C	4512	687	.1523
CH₂	4871	671	.1378
C	4135	646	.1562
CH₂	4609	649	.1408
Out	1481	361	.2438
$23\frac{1}{2}$" Pb	2571	5.2	.0020
C	2717	433	.1594
CH₂	4901	660	.1347
C	4165	643	.1544
CH₂	4804	651	.1355
C	5124	776	.1514
CH₂	14465	1996	.1380
C	4301	654	.1521
CH₂	3081	420	.1363
C	4173	644	.1543
CH₂	4772	643	.1347
C	4283	647	.1511
Out	4801	1183	.2464

	Average	C	.1538
		CH₂	.1369

Sample thicknesses

C   25.47 gm/cm²

CH₂   29.74 gm/cm²

$$\sigma_H = 391 \ln \frac{1538}{1369} = 45.6 \text{ MB}$$

Analysis of data

	C	CH₂
$\frac{1}{R_m}\sqrt{\frac{\Sigma\,(R_i - R_m)^2}{N-1}}$	.018	.015
Expected Standard Deviation (Statistics only) . . .	.015	.015

Table 2 - Summary of C-CH$_2$ and D$_2$O-H$_2$O Results

Run	Thickness of Carbon (H$_2$O) in M.F.P.	θ	Measured σ (10^{-27} cm^2)	Background Correction (10^{-27} cm^2)	Observed S.D. (10^{-27}cm^2)	Expected S.D. (Statistics only) (10^{-27}cm^2)
I C-CH$_2$ Difference						
7-24	0.56	0.66°	45.6	+ 0.2	3.6	3.3
7-30	1.02	0.68°	41.0	0.2	1.8	1.8
2-5	0.56	0.66°	47.3	0.5	6.3	3.5
II D$_2$O - H$_2$O Difference						
7-25	1.09	0.67°	44.7	+ 0.2	2.2	2.2
7-29	1.09	1.5°	39.7	0.2	2.0	2.0

III Weighted Averages Including Estimate of Systematic Error

Total cross sections for 1.4 Bev neutrons:

$$\sigma_H = 42.4 \pm 1.8 \text{ MB}$$

$$\sigma_D - \sigma_H = 42.2 \pm 1.8 \text{ MB}$$

slightly in the second D_2O - H_2O run by increasing the angle subtended by the detector to 1.5°. Table 2 summarizes the results of five runs and gives the weighted average value with the estimated error. The mean effective neutron energy for this experiment is taken to be 1.4 ± 0.2 Bev. This result is calculated from the half-width of the observed angular distribution of diffraction-scattered neutrons from C, Cu, and Pb and is discussed in more detail in the next section.

Absorption and Total Cross Sections for Be, C, Al, Cu, Sn, Pb, Bi, U and the Integral Angular Distribution of Diffraction-scattered Neutrons

The eight elements Be ..... U were chosen for this experiment because they are conveniently spaced through the periodic table (except Pb and Bi) and are readily available. Samples of each of these elements were made to be about one half an absorption length in thickness; this choice is a compromise between the most efficient length for cross section measurements and the thin scatterer which minimizes multiple diffraction scattering effects.

The experimental arrangement as shown in Figure 11 is the same as described in the last section, except that the neutron beam is collimated to a 1" diameter. The detector is displaced horizontally and vertically until the maximum counting rate is obtained and then is held fixed.

The scatterer is placed at various distances from 6" to 30' from the detector so that θ, the half angle subtended, ranges from $12°$ to $0.2°$. Data is collected by changing the scatterer or the geometry after about 2500 counts are recorded; following every three or four such changes, 2500 counts are taken with the scatterer removed.

For the three elements C, Cu, and Pb the transmission was measured at several angles between $0.2°$ and $12°$. The results are collected in Figures 12, 13, and 14 which show the measured values before and after a correction for instrumental effects described in a later section.

The transmission measured in "good" geometry (θ = 0.2 to $0.5°$) corresponds to the total nuclear cross section, σ_T; in bad geometry (θ = 6 to $10°$) practically all of the diffraction-scattered particles are collected hence the transmission corresponds to the absorption cross section, σ_A. We have taken the shape of the integral angular distribution given by the optical model and fitted it to the data by adjusting three parameters, σ_T, σ_A and kR; σ_T is fixed by the intercept $T(0°)$, σ_A is fixed by the "plateau" value, and kR by the angular width of the diffraction pattern. For simplicity, the optical model distribution of Equation 4.4 was taken setting $k_1/K = 0$ and $KR = 3$. The analysis of Chapter IV derives the nuclear radius for C, Cu, and Pb from the value of σ_A; taking these radii, the single value $k = 10.2 \times 10^{13} cm^{-1}$;

- 18 -

TRANSMISSION VERSUS θ FOR CARBON (25.47 GM/CM^2)

Figure 12

TRANSMISSION

.80

.70

.60

.55

3.3°

○ MEASURED VALUE

● CORRECTED VALUE AND
RANDOM ERROR

—— THEORETICAL VALUE
FOR: σ_T =380 MB
σ_A =205 MB
kR =29, T=1.4 BEV

0   2   4   6   8   10   12   14   16   18   20

θ (DEGREES)

Figure 13

TRANSMISSION VERSUS θ FOR COPPER (43.40 GM/CM^2)

O MEASURED VALUE

● CORRECTED VALUE AND
RANDOM ERROR

—— THEORETICAL VALUE
FOR: σ_T = 1340 MB
σ_A = 670 MB
kR = 50, T=1.4 BEV

TRANSMISSION

θ (DEGREES)

2°

TRANSMISSION VERSUS θ FOR LEAD (89.78 GM/CM^2)

○ MEASURED VALUE
● CORRECTED VALUE AND RANDOM ERROR
— THEORETICAL VALUE
FOR: σ_T =3210 MB
σ_A =1730 MB
kR =77.5, T=1.4 BEV

1.25°

TRANSMISSION

θ (DEGREES)

Figure 14

is chosen to fit the data of figures 12, 13, and 14. This value corresponds to a mean effective neutron energy of 1.4 Bev. An accurate estimate of the mean effective energy cannot be gotten in this way but values outside the range 1.2 to 1.6 Bev are excluded by the data.

The theoretical curves plotted in figures 12, 13, and 14 are the prediction for a monoenergetic beam of 1.4 Bev neutrons; to what extent this will be modified by a spectrum of neutron energies can be estimated from Figure 15 which shows the integral angular distribution predicted for 1.4 Bev neutrons and for a mixture of 1.0 and 2.2. Bev neutrons having the same mean energy. The reasonably good agreement indicates that this method yields approximately a linear average of the neutron energy over the energy spectrum involved.

The same experimental arrangement was used to measure the attenuation of the remaining five elements Be, Al, Sn, Bi, and U but these were done in good (0.55^{o}) and bad geometry (6.0^{o}) only. Much of the later data was obtained with a modified version of the neutron detector; that is, the last counter in the four-fold telescope was replaced with a scintillator 6" in diameter, and the third counter, C_3 was replaced with a 4" scintillator. The 6" lead absorber was divided into a $1\frac{1}{2}$" piece between C_1 and C_2, a $1\frac{1}{2}$" piece between C_2 and C_3 , and a 3" piece between C_3 and C_4. With this change, the half-angle subtended by the 4-fold telescope at the aluminum radiator

- 19 -

CALCULATED EFFECT OF NEUTRON ENERGY SPECTRUM
ON ANGULAR DISTRIBUTION

$$F = \frac{1}{\sigma_p} \int \frac{d\sigma_p}{d\theta} d\theta$$

—— $F(k_{1.4}R\theta)$ FOR 1.4 BEV NEUTRONS ONLY

———— $1/3 \left\{ 2F(k_{1.0}R\theta) + F(k_{2.2}R\theta) \right\}$
FOR MIXTURE OF 1.0 AND 2.2 BEV
NEUTRONS HAVING MEAN ENERGY 1.4 BEV

$k_{1.4}R\theta$
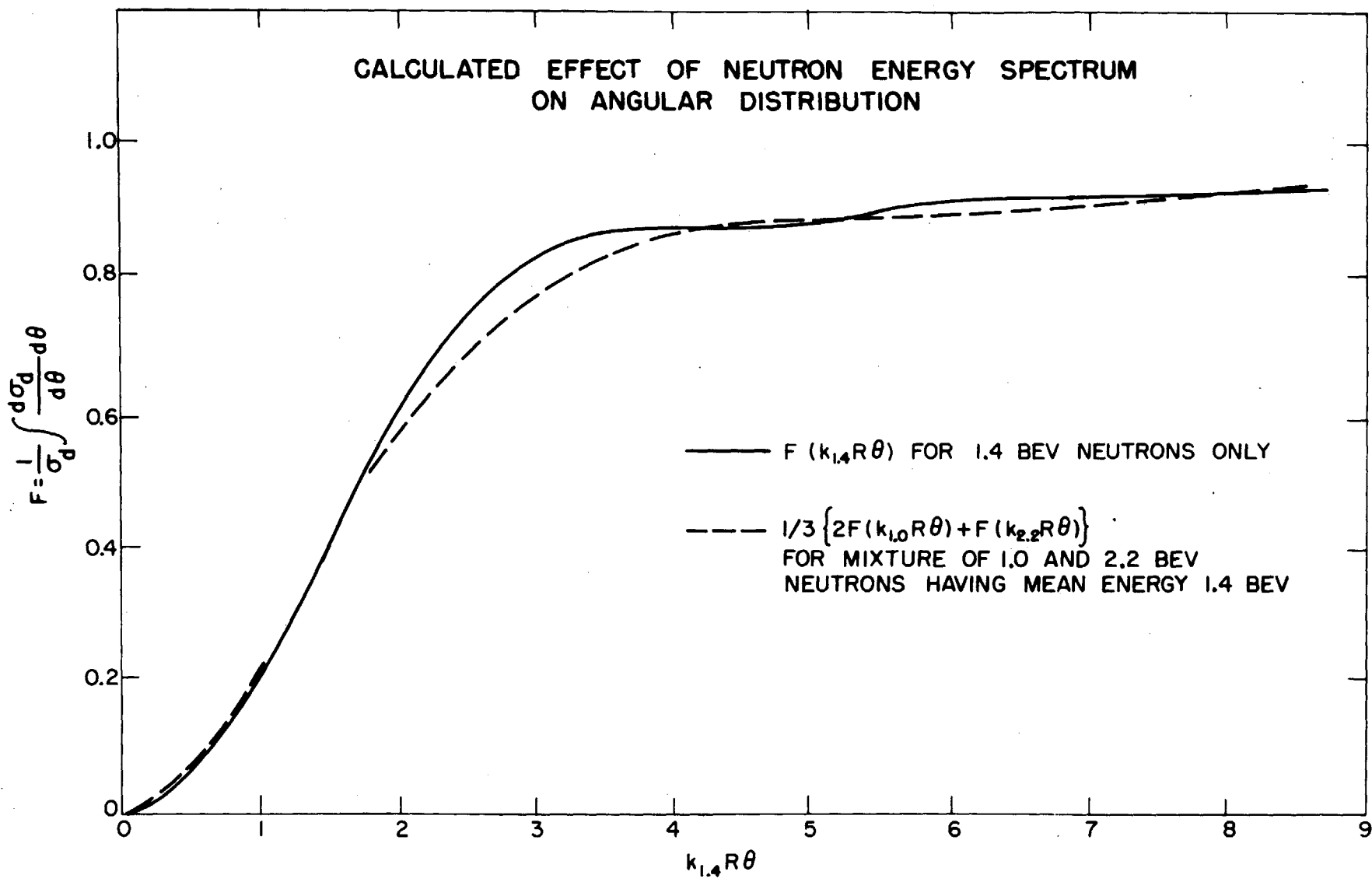
Figure 15

is increased from 4.3° to 15° and the detection efficiency is increased by a factor of about three.

In order to extract the values of σ_A and σ_D; the corrected values of transmission are converted to cross sections and inserted in equations of the form

$$\sigma(\theta) = \sigma_A + \left[1 - F'(\theta)\right]\sigma_D$$

in which $\sigma(\theta)$ is the measured value of cross section at half angle θ. $F.(\theta)$ is the fraction of the scattering angular distribution contained in a cone of half angle, θ:

$$F'(\theta) = \frac{1}{\sigma_D} \int_0^{\theta} \frac{d\sigma_D}{d\omega} \, d\omega$$

$F(\theta)$ is calculated from the angular distribution for single scattering (Equation 4.4) assuming $k_1/K = 0$, $k = 10.2 \times 10^{13}$ cm^{-1} and an approximate value of R. In the limits of good or bad geometry, $F(\theta)$ is near 0 or 1 respectively and insensitive to the values chosen for kR. For each of the elements Pb, Cu, and C for which many points were measured, the equations obtained for θ in the range 0.2° to 0.7° are averaged to obtain one condition on σ_A and σ_D; the equations for θ in the range $6 - 10^{\circ}$ are averaged to obtain a second condition from which σ_A and σ_D are then determined. The values obtained from intermediate geometries are ignored because these are sensitive to multiple scattering corrections, uncertainties in kR, effects of the neutron energy spectrum and uncertainties in the correction. For the remaining five

elements, only good and bad geometry measurements were made, σ_A and σ_D being determined from the resulting two equations.

The basic data for the eight elements Be .... U are contained in Table 3. This table lists the transmission measured at each subtended angle, the corrections applied to the data, the corrected cross sections for each angle, and the resulting equations and values for the absorption and scattering cross sections.

Corrections and Errors

There are two instrumental effects which introduce an important systematic error in the poor geometry measurements and for which a correction to the data has been made:

Directionality of the Detector

The arrangement of the detector is such that the efficiency of detection is dependent on the angle which the incident neutron makes with the axis of the detector. In general, the scattered neutrons which enter the detector in a diverging cone are counted with reduced efficiency relative to the unattenuated neutrons which enter parallel to the axis. The dependence of the detection efficiency on angle was measured directly by observing the counting rate as the detector is inclined at various angles to the collimated beam, the radiator remaining fixed in the beam. The result is the angular distribution of penetrating secondaries produced in aluminum (shown in Figure 8). This

shows, for example, that the detection efficiency falls off to half maximum for neutrons entering the detector at an angle of 11° to the axis. The correction to the observed transmission at a given half angle is computed by averaging the measured relative efficiency over an approximate angular distribution (up to the angle θ) then increasing that portion of the observed transmission which is due to scattered particles, $T(\theta) - T(0)$, to compensate for the reduced efficiency. The correction is largest for the light elements: it amounts to 24% of σ_A in carbon, 6% of σ_A in lead. In good geometry the correction becomes negligible and hence does not affect σ_T. Appendix B discusses the calculation in more detail.

Finite Beam Size

In this experiment, the diameter of the collimated beam (1") is not negligibly small compared to the aperture of the detector ($2\frac{1}{2}$" diameter) therefore account must be taken of the fact that the probability, g, that a particle scattered through an angle, ξ , shall enter the detector depends upon ξ , upon the half angle of collection θ, and upon the distance , ρ , from the axis at which the scattering occurs. Under the simplifying assumption that the detector efficiency is independent of angle and uniform over the $2\frac{1}{2}$" aperture, the detector probability, g, is suitably averaged over an approximate angular distribution

and over the cross section of the incident beam. Then a compensating correction is made to relate the observed transmission to the idealized case of a collimated beam of zero width; the correction to the transmission amounts at most to 6% of the contribution from scattered particles, $T(\theta) - T(0^\circ)$, in the region where T vs θ is rapidly rising. The correction is the same for all elements at corresponding points of the diffraction pattern and vanishes in both good and bad geometry limits in all cases. Details of the calculation are given in Appendix C.

Table 3

Measured Transmission, Corrections, and Derived Values

of σ_A and σ_D

Explanation of Symbols

> W   The statistical weight of each measurement.
> The fractional standard deviation in T
> (due to statistics only) is given by:
>
> $$S. D. = \frac{.044}{\sqrt{W}}$$
>
> Θ The half angle subtended by the detector at
> the scatterer
>
> T, T^1 The measured and corrected transmission
>
> C_1, C_2 Correction factors (see text)

During the experiment the detector was modified by
replacing the last counter with one 6" in diameter.
The last two counters were replaced later by 4" and
6" counters. The data taken with these modifications
are listed under the headings Mod. Det - 6 and Mod.
Det. -4, 6 respectively.

All cross sections are in units of 10^{-27} cm^2.

Table 3.1

Beryllium

18.80 gm/cm^2

$$\sigma = 796.4 \ln \frac{1}{T}$$

W	θ	T	$T-T_0$	C_1	C_2	T^1	Aver T	σ
37	0.55°	.681	0			.681		306
16	3.	.706	.025	1.15	1.04	.711		271
36	6.	.741	.060	1.25	1.06	.761	776	202
8	8.	.748	.067	1.24	1.03	.767		210
3	10.	.761	.080	1.22	1.014	.780		197

Mod. Det. - 4, 6

W	θ	T	$T-T_0$	C_1	C_2	T^1		
20	6.	.773	.092	1.18	1.06	.796		

W	θ	σ = σ_A + (1 - F)σ_D		
56	6°	202 = σ_A +	.135 σ_D	
8	8	210 =	.11	
3	10	197 =	.10	

Average (10°)		203 = σ_A + 0.13 σ_D		(1)
	0.55°	306 = σ_A + 0.98 σ_D		(2)

Result

$$\sigma_A = 187$$
$$\sigma_D = 121$$

Table 3.2

Carbon

25.47 gm/cm^2
$\qquad\qquad\qquad\qquad\qquad\qquad$ $\sigma = 783 \ln \frac{1}{T}$

W	θ	T	T-T$_0$	C$_1$	C$_2$	T^1	Aver T^1	σ
12	0.55°	.614	-			.614		382
93	0.67	.625	.005	1.067	1.007	.625	.624	370
12	1.55	.644	.024	1.095	1.019	.647		341
4	2.3	.659	.039	1.125	1.029	.665		320
12	3.0	.654	.034	1.15	1.042	.661		322
8	4.0	.706	.086	1.19	1.056	.728		248
8	5.0	.700	.080	1.23	1.061	.725		252
26	6.0	.7155	.0955	1.25	1.06	.747	743	234
20	8.0	.7235	.1035	1.24	1.033	.753	758	217
11	10.	.735	.115	1.22	1.014	.763		211
4	13.	.730	.110	1.20	1.01	.763		211

Mod. Det —6

W	θ	T	T-T$_0$	C$_1$	C$_2$	T^1
6	0.66	.615	—			.615
7.5	8.0	.744	.124	1.20	1.033	.774

Mod. Det. —4, 6

W	θ	T	T-T$_0$	C$_1$	C$_2$	T^1
12	0.66	.616				.616
11	6.	.710	.090	1.18	1.06	.733
12	8.	.732	.112	1.17-	1.033	.756

W	θ	σ	=	σ$_A$	+	(1 - F)	σ$_D$	D
12	0.55	382	=	σ$_A$	+	0.97	σ$_D$	
111	0.67	370	=			0.96		
	(Aver)	371	=	σ$_A$	+	0.961	σ$_D$	(1)
37	6	234	=	σ$_A$	+	0.147	σ$_D$	
39	8	217	=			0.11		
11	10	211	=			0.10		
	(Aver)	223	=	σ$_A$	+	0.124	σ$_D$	(2)

Result

$\sigma_A = 201$

$\sigma_D = 177$

Table 3.3

Aluminum

41.20 gm/cm^2 $\qquad\qquad\qquad\qquad$ $\sigma = 1086 \ln \frac{1}{T}$

W	θ	T	T - T_o	C_1	C_2	T^1	σ
8	0.21^o	.521	0			.521	707
17	0.55^o	.532	.011	1.065	1.007	.533	685
9	3	.585	.064	1.135	1.056	.598	557
17	6	.643	.122	1.150	1.033	.666	446

W	θ	σ	=	σ_A	+	(1 - F)	σ_D	
	0.21	707	=	σ_A	+	0.99	σ_D	
	0.55	685	=			0.96		
(Aver)		696	=	σ_A	+	0.975	σ_D	(1)
	6.0	446	=	σ_A	+	0.11	σ_D	(2)

Result

$$\sigma_A = 414$$
$$\sigma_D = 289$$

Table 3.4

Copper

43.40 gm/cm^2

$$\sigma = 2431 \ln \frac{1}{T}$$

W	θ	T	T-T$_o$	C$_1$	C$_2$	T^1	Aver T^1	σ
8	0.21°	.567	.004	1.055	1.003	.567		1321
11	0.55	.570	.007	1.065	1.01	.571	.5695	1372
20	1.5	.618	.055	1.095	1.033	.625		1142
8	2.	.665	.102	1.112	1.048	.682		929
4	2.5	.657	.094	1.126	1.058	.675		952
22	3.	.6735	.1105	1.136	1.063	.697		875
19	4.	.698	.135	1.142	1.052	.726		776
31	6.	.712	.149	1.119	1.014	.732	.728	770
30	8.	.736	.173	1.112	1.008	.757		675
16	10.	.710	.147	1.107	1.006	.727		774
8	12.	.716	.153					

Mod. Det. - 4, 6

W	θ	T	T-T$_o$	C$_1$	C$_2$	T^1		
10	0.55	.568	.005	1.06	1.01	.568		
11	6.	.704	.141	1.088	1.014	.718		

W	θ	$\sigma = \sigma_A + (1 - F)\sigma_D$		
8	0.21	1321 = σ_A +	0.988	σ_D
21	0.55	1372 =	0.950	
(Aver)		1360 = σ_A +	0.959	σ_D
42	6	770 = σ_A +	0.110	σ_D
30	8	675 =	.075	
16	10	774 =	.065	
(Aver)		739 = σ_A +	.091	σ_D

Result

$$\sigma_A = 674$$

$$\sigma_D = 714$$

Table 3.5

Tin

62.62 gm/cm^2

$$\sigma = 3146 \ln \frac{1}{T}$$

W	θ	T	T-T$_o$	C$_1$	C$_2$	T^1	σ
8	0.21°	.497				.497	2200
9	0.55	.512	.008	1.065	1.011	.512	2105
9	3	.628	.124	1.100	1.057	.647	1369
17	6	.660	.156	1.075	1.009	.673	1242

W	θ	σ =	σ_A +	(1 - F) σ_D	
8	0.21	2200 =	σ_A +	0.98	σ_D
9	0.55	2105 =		0.925	
(Aver)		2153 =	σ_A +	0.953	σ_D (1)
	6	1242 =	σ_A +	0.08	σ_D (2)

Result

$$\sigma_A = 1158$$

$$\sigma_D = 1044$$

Table 3.6

Lead

89.78 gm/cm^2　　　　　　　　　　　　　　　$\sigma = 3830 \ln \frac{1}{T}$

W	θ	T	$T-T_0$	c_1	c_2	T^1	Aver T	σ
13	0.21°	.435	.003	1.055	1.006	.435		3185
19	0.55	.453	.021	1.065	1.016	.455	.455	3020
15	1.15	.572	.080	1.087	1.042	.522		2485
15	1.75	.558	.126	1.095	1.061	.579		2100
15	2.3	.580	.148	1.093	1.060	.604		1930
17	3.0	.593	.161	1.085	1.037	.614		1870
26	4.5	.629	.197	1.07	1.01	.645		1680
31	6.	.624	.192	1.063	1.007	.640	.618	1850
8	8.	.650	.218	1.06	1.005	.666	.630	1770
8	10.	.645	.213	1.056	1.005	.657	.634	1750
8	12.	.641	.209	1.052	1.005	.652		1632

Mod. Det - 6

W	θ	T	$T-T_0$	c_1	c_2	T^1	Aver T	σ
6	0.55	.478	.046	1.05	1.016	.481		
14	6.	.617	.185	1.056	1.007	.627		

Mod. Det. - 4, 6

W	θ	T	$T-T_0$	c_1	c_2	T^1	Aver T	σ
12	0.55	.440	.008	1.045	1.016	.441		
48	6.	.595	.163	1.047	1.007	.603		
20	8.	.608	.176	1.042	1.005	.616		
9	10.	.603	.171	1.042	1.005	.611		

Table 3.6

Lead - (Continued)

W	e	σ =	σ_A	+	$(1 - F)\sigma_D$	
13	0.21	3185 =			0.975 σ_D	
37	0.55	3020 =			0.875	
	(Aver.)	3061 =	σ_A	+	0.90 σ_D	(1)
93	6	1850 =	σ_A	+	.073 σ_D	
28	8	1770 =			.050	
17	10	1750 =			.040	
	(Aver.)	1822 =	σ_A	+	0.064 σ_D	(2)

Result

$$\sigma_A = 1727$$

$$\sigma_D = 1482$$

<div align="center">

Table 3.7

</div>

Bismuth

87.18 gm/cm^2 $\qquad\qquad\qquad\qquad\qquad$ $\sigma = 3979\ \ln\frac{1}{T}$

W	θ	T	$T-T_0$	C_1	C_2	T^1	Aver T'	σ
13	0.55°	.468	.018	1.065	1.016	.469		
8	6.	.622	.172	1.063	1.007	.634		
			Mod. Det. — 4, 6					
25	0.55	.456	.006	1.045	1.016	.456	.460	3090
25	6.	.610	.160	1.047	1.007	.618	.622	1890
20	8.	.618	.168	1.042	1.005	.626		1860
8	10.	.608	.158	1.042	1.005	.616		1920

W	θ	$\sigma =$	σ_A	+	$(1 - F)$	σ_D	
33	6	1890 =	σ_A	+	.073	σ_D	
20	8	1860 =			.050		
8	10	1920 =			.040		
	(Aver.)	1882 =	σ_A	+	.060	σ_D	(1)
	0.55	3090 =	σ_A	+	.875	σ_D	(2)

Result

$$\sigma_A = 1793$$

$$\sigma_D = 1482$$

Table 3.8

Uranium

72.57 gm/cm^2

$$\sigma = 5445 \ln \frac{1}{T}$$

W	θ	T	$T-T_o$	C_1	C_2	T^1	Aver T^1	σ
14	0.55°	.525				.527	.531	3430
14	6.	.679	.169	1.061	1.007	.691		2010

Mod. Det. — 4, 6

W	θ	T	$T-T_o$	C_1	C_2	T^1		
11	0.55	.535				.537		
11	6.	.682	.172	1.045	1.007	.691		

W	θ	σ	=	σ_A	+	$(1-F)\sigma_D$		
	0.55	3430	=	σ_A	+	0.88	σ_D	(1)
	6.	2010	=	σ_A	+	0.07	σ_D	(2)

Result

$$\sigma_A = 1887$$
$$\sigma_D = 1753$$

Several other possible sources of systematic and random errors have been considered of which the most important are the following:

1. Random Errors

In the $C-CH_2$ and D_2-H_2O difference experiments, each day's run consists of about 10 groups of 5,000 counts each on each sample. The observed r.m.s. deviation from the mean of the ten groups ranges from 1.0 to 1.8 times the deviation expected from statistical fluctuations only. The excess fluctuation is significant and may arise from instability of the electronic equipment or it may reflect the variable operating conditions of the Cosmotron since the beam which is monitored (3° from the forward direction, some charged particles counted) may not be completely correlated with the neutron beam which is directly used (1^O from the forward direction).

For the transmission measurements on the elements Be, C, ... U, all the data obtained over a six month period was analyzed for fluctuations from the mean value. The observed r.m.s. deviations are, on the average, about 1.6 times the expected deviation due to statistics only.

2. Rate Effects

A systematic error can arise if the detection and counting system has a non-linear response to the flux of incident neutrons. Chance coincidences or dead-time

effects in the coincidence or scaling circuits can cause such a non-linearity. An experimental estimate of chance coincidences was gotten by delaying the signal from one counter by ($2\frac{1}{2}$ x 10^{-8} seconds) or about three times the resolving time. The contribution of accidentals is about 0.8% of the normal counting rate. The main contribution to accidentals in the four-fold coincidence telescope is probably "true" three-fold events in the first three counters in chance coincidence with a spurious count in the last counter. Using approximate values for the average triple and single rates, the expected effect is several times smaller than 0.8%, however, the beam intensity is not uniform during each pulse and undoubtedly reaches peak values of several times the average. If the contribution of accidental counts is taken to be of the order of 0.8% and this effect is assumed to vary quadratically with the beam intensity (experimentally the dependence is found to be more nearly linear) the effect would make the observed transmission systematically too large by about 0.3%.

The counting losses due to dead-time in the discriminator and scaling circuits should be negligible since the average four-fold rate is about one count per 10^{-3} seconds during the pulse and the measured dead-time is 2 x 10^{-7} seconds.

The possibility was considered that charged secondaries originating in the scatterer may enter the

anti-coincidence counter and thus cause a dead-time effect.
To test this, the anti-coincidence counter was exposed
to a heavy flux of charged particles from an independent
beam and the four-fold rate observed with the anti-coincid-
ence counter connected and disconnected. No dead-time
effect was observed within a statistical uncertainty of 2%.

In the normal course of operation data was taken
with beam intensities varying over a range of about 10 to
1. Analysis of the measured values of transmission show
fluctuations in excess of statistics but the deviations
from the mean value do not appear to be correlated with
the beam intensity. However, effects of the order of 1%
or less cannot be excluded.

3. Charged Particles

The presence of charged particles in the neutron
beam caused the observed counting rate to increase by about
50% when the anti-coincidence counter is disconnected.
(The ratio of charged particles to neutrons in the beam
is of the order of 0.1%; the effect is large because of
the poor efficiency for detecting neutrons of about 0.1%).
The measured efficiency of the anti-coincidence counter is
0.99 or greater, therefore, the maximum effect due to
charged particles is about 0.5% of the measured transmission.
The maximum effect is realized in the good geometry
measurements on the heavy elements; in this case the

charged particles are almost completely removed from the detected beam due to Coulomb scattering. In the poor geometry measurements the effect is probably negligible since the absorption cross-section for the charged particles if they are protons or pions is presumably not much different than that for neutrons.

4. Background

A small residual count is observed when the neutron beam is completely attenuated. This background is probably due to minor leaks in the shielding and scattering from adjacent ports. When the neutron beam is attenuated with a column of lead 3" wide and 52" thick we observe a residual counting rate of about 0.4% of normal. The effect of this is to make the observed transmissions systematically too large by about 0.2%.

5. Gamma Rays

A high energy gamma ray component of the beam is expected to arise from the decay of π^0 mesons produced in the Cosmotron target. However, to register in the detector would require a gamma ray to produce a shower capable of penetrating six inches of lead (27 radiation lengths). To produce a shower with one electron remaining at this depth requires, on the average, an incident photon of about 50 Bev. Furthermore, a $1\frac{1}{2}$" lead filter (6.7 radiation lengths) is placed in the beam between the target

and the collimator (see Figure 10) to intercept low energy
charged particles and gamma rays. The effect of gamma rays
is believed to be negligible.

6. Secondaries

The fact that a plateau in the transmission is
observed in poor geometry for Pb, Cu, (and less strikingly
for C) suggests that secondary neutrons from inelastic
processes do not make a major contribution to the observed
counting rate. An estimate of the importance of neutral
secondaries (above the detector threshold) might be made
from the production cross section for <u>charged</u> secondaries
(of comparable energy) which was measured in the same neutron
beam. (See Chapter II). The nuclear cross sections for
producing energetic neutral secondaries is probably smaller
than that for producing energetic charged secondaries
since the latter include mesons as well. The measured
production cross sections, $\sigma_s(4°)$, are extrapolated
to $\sigma_s(8°)$ on the basis of the measured angular distribution.
The values of the nuclear absorption cross section are
listed for comparison; the values $\sigma_s(8°)$ probably re-
present an upper limit to the error in σ_A due to the
detection of neutral secondaries.

7. Multiple Scattering

Concerning the carbon-polyethylene difference
method of measuring σ_H , it is clear that in the limit

- 28 -

Table 4

Data on Production of Charged Secondaries by Neutrons

Convertor	Be 2" thick	Be 4"	Al 2"	Pb 2"
Measured $\sigma_s(4^\circ)$ in millibarns	3.9	3.5	8.2	12.5
Extrapolation $\sigma_s(8^\circ)$ in millibarns	6.8	6.1	14	22
$\dfrac{\sigma_s(8^\circ)}{\sigma_A}$	-	.034	-	.034	.012

$\sigma_s(4^\circ)$ is the measured cross section for production of penetrating (6" Pb) charged secondaries within 4° of the forward direction by neutrons of energy $1 - 2.2$ Bev. The absolute magnitudes are uncertain by about a factor of two, the relative values are accurate to 5%.

of good geometry any incident neutron which interacts
with either a carbon or a hydrogen nucleus is removed from
the detected beam. (This is, of course, the definition of
good geometry). In our approximations to good geometry
($\theta = 0.7^\circ$) it is necessary to consider two questions:

(1) What contribution to the detected beam is made by
     single and multiple diffraction scattering in the
     carbon sample?

(2) How much are these contributions modified by the
     presence of hydrogen in the polyethylene sample?

To discuss these effects, it is convenient to express the
angular distribution expected from a scattering sample
of finite thickness in the following way (See Ref (10)
and Appendix A):

$$(3.3) \quad N(\theta) = N_0 \, \epsilon^{-\ell\sigma_T} + N_0 \, \epsilon^{-\ell\sigma_A} \sum_1^\infty \frac{1}{n!} (\ell\sigma_D)^n \epsilon^{-\ell\sigma_D} F_n(\theta)$$

where N (θ) =   number of particles emerging from sample
                        within cone of half angle θ.

N_0 =   number of particles incident

ℓ =   number of nuclei per unit area

$F_n(\theta)$ =   fraction of n-fold scattered particles con-
                   tained in a cone of half angle θ. For the
                   present purpose the approximation

$$F_n(\theta) = F_1\left(\frac{\theta}{\sqrt{n}}\right)$$

is used.

In equation (3.3) the Poisson factor, $\frac{1}{n!}(\ell\sigma_D)^n \epsilon^{-\ell\sigma_D}$

expresses the probability that an incident particle would

be scattered exactly n times in the thickness ℓ if there

were no absorption. The n-th term, $N_0 \epsilon^{-\ell\sigma_A} \frac{1}{n!}(\ell\sigma_D)^n$

$\times \epsilon^{-\ell\sigma_D} F_n(\theta)$ represents the number of particles that are

scattered exactly n-times, do not suffer absorption, and

emerge within a cone of half angle θ. Taking an approxi-

mate angular distribution for 1.4 Bev neutrons diffraction-

scattered from carbon:

$$\frac{d\sigma_D}{d\omega} \simeq \frac{\sigma_D}{2\pi\eta_c^2} \epsilon^{-\frac{\theta^2}{2\eta_c^2}}$$

$$\eta_c = 2.5^\circ$$

(Valid for
small angles)

and the values of ℓ and θ for a typical carbon sample

and geometry, equation (3.3) becomes:

$$N(\theta) = N_0 \epsilon^{-\ell\sigma_T}\left[\underbrace{}_{} \quad + \underbrace{.0070}_{} \quad + \underbrace{.0043\cdots}_{}\right]$$

Relative contribution   Non-interacting   Single   Double
                   from: particles   Scattering   Scatter-
                                                                        ing

The contribution from single and multiple scattering in

carbon is seen to be small; in the polyethylene sample

containing the same amount of carbon these contributions are

reduced by about 10% since there is about 0.1 m.f.p. of

hydrogen present and essentially every interaction with

hydrogen removes the neutron from the detected beam. Hence, the difference in multiple scattering effects in the two cases is negligible. Almost the same estimates apply to the measurement of $\sigma_D - \sigma_H$ by the D_2O-H_2O difference.

For the eight elements Be through Pb the cross sections measured at each angle were fitted with the angular distribution for single scattering. The error introduced by multiple diffraction scattering can be estimated by comparing the expression (3.3) with the usual expression for exponential attenuation:

$$(3.4) \quad N(\theta) = N_0 e^{-\ell(\sigma_T - F_1'\sigma_D)}$$

$$N(\theta) = N_0 e^{-\ell\sigma_T}\left\{ 1 + \sum_1 \frac{1}{n!}(\ell\sigma_D)^n F_1'^n \right\}$$

Equation (3.4) already takes approximate account of multiple scattering by including in the nth term the single scattering distribution raised to the n-th power, F_1^n, instead of the correct distribution for n-fold scattering.

For the angular distribution of interest in this experiment the approximation is a fair one: for example, $(F_1)^2$ is a distribution about 50% broader than the single scattering distribution F_1. It is not identical in shape with the correct function F_2 but has the same general features. Combining (3.3) and (3.4), the cross section $\sigma(\theta)$

measured at an angle θ can be expressed as:

$$(3.5) \quad \sigma(\theta) \simeq \sigma_A + (1 - F_1) \sigma_D$$
$$- \sigma_D \left\{ \epsilon^{-\rho \sigma_D F_1} \sum_2 \frac{1}{n!} (\rho \sigma_D)^{n-1} (F_n - F_1^n) \right\}$$

The first two terms on the righthand side are the single scattering approximation which is used to fit the data; the term in brackets is the correction due to multiple scattering effects. The correction term vanishes both in the good and bad geometry limits; it vanishes at all angles in addition for very thin scatterers. Using the method of Appendix A to calculate the function F_n, the correction to the cross section is about $\frac{1}{2}\%$ for the scatterer thickness and geometries of this experiment.

8. "Scattering In"

The $C-CH_2$ and D_2O-H_2O difference experiments were done in good geometry using a collimated beam 2" in diameter. Because the incident beam diverges slightly a small portion of it (an estimated 7%) misses the detector unless scattered through the appropriate angle upon traversing the scatterer. However, due to the very small solid angle subtended by the detector, this effect contributes less than .5% to the observed counting rate for a typical carbon sample and is thus negligible.

In the transmission measurements of Be, C ... U

a 1" collimated beam was used so that the entire beam strikes the detector when the scatterer is removed so that "Scattering in" is not a factor.

9. Errors in Correction

The correction for the directionality of the telescope is sizeable for the poor geometry measurements of the light elements and the uncertainties in this correction are difficult to estimate but are taken, somewhat arbitrarily, as $\pm$ 20%.

10. Finite Scatterer Thickness

In the poor geometry measurements, the thickness, t, of the scattering sample is an appreciable fraction ($\sim$ 1/3) of the distance, ℓ , from the sample to the detector there- fore, the half angle, θ, for collection is poorly defined. To correct the observed values of transmission to the ideal- ized case of zero scatterer thickness and perfectly defined geometry, an approximate integral angular distribution is suitably averaged over the thickness, t, of the scatterer. The magnitude of this correction to the observed transmission is less than 0.6% in all cases and has been neglected; the effect is small for two reasons: (1) the integral angular distribution in bad geometry (for example, the plateau region of Figure 12) is only a slowly varying function of θ and (2) since the distance ℓ is measured from the center of the sample and the appropriate average over the scatterer

thickness is a linear average, the correction is second
order in (τ / ℓ).

11. Impurities, etc.

The samples of polyethylene used were molded from
high purity commercial powder. The samples chosen are free
from air bubbles and the measured density is 0.922 $\pm$ .001
which is within 0.1% of the established value. The im-
purities are believed to be negligible for this experiment.
The carbon samples are blocks of reactor-grade graphite of
extreme purity. The thickness in grams per cm^2 was
measured to within 0.5%; this uncertainty can introduce
an error of 0.25% of the carbon cross section or 0.9 mb.

The matched samples of heavy water - ordinary
water are believed to contain negligible impurities and the
thicknesses are known to an estimated $\frac{1}{2}$%; the corresponding
uncertainty in the n-n cross section is 1.0 mb.

The samples of the eight elements Be - Pb, were
carefully weighed and measured so that the thickness in
grams/cm^2 is known to within $\frac{1}{2}$%. The effect of possible
impurities is believed to be negligible in all cases.

Summary and Treatment of Error

In the measurement of the hydrogen and deuterium
cross sections the dominant error arises from the random
fluctuations as described in Section 1 above. The observed
r.m.s. standard deviations for each run are converted to

standard deviation in cross section. These are listed in Table 2. A minor correction is made for background.

The errors in measuring the transmission of the elements Be, C ... U are composed of:

a) An error due to random fluctuation which is taken as 1.6 times the expected s.d. due to statistics only.

b) An uncertainty of 1% to include the effects of background, charged particles, and possible rate effects.

c) An uncertainty in the correction for directionality of 20% of its value.

The contributions from a, b, and c are listed in Table 5. They are combined as random errors, the resultant error in transmission is listed in column 4, and corresponding error in cross section in column 5.

It should be noted that these uncertainties in the absorption cross section do <u>not</u> include the possible effect of:

d) Detection of neutral secondaries from inelastic processes. The estimates given in Table 4 are probably upper limits to this effect.

e) Uncertainties in the theoretical angular distribution which is used to extrapolate the measured cross sections.

Table 5

Composition of Errors

	Percentage Error in T				in σ_A	in R
due to:	Random Errors	Un-certainty in C_1, C_2	Rate Effects, Charged Particles, Etc.	Re-sultant		

(POOR GEOMETRY)

Be	1.0	0.6	1.0	1.5	6.4	7.0
C	0.8	0.9	1.0	1.6	6.2	4.8
Al	1.7	0.6	1.0	2.1	5.5	3.7
Cu	0.8	0.5	1.0	1.4	5.0	2.8
Sn	1.7	0.4	1.0	2.0	5.4	2.9
Pb	0.6	0.3	1.0	1.2	2.6	1.4
Bi	1.0	0.3	1.0	1.4	3.1	1.7
U	1.4	0.3	1.0	1.8	5.2	2.8

				in T	in σ_T

(GOOD GEOMETRY)

Be	1.2	0.0	1.0	1.6	4.2
C	0.7		1.0	1.2	2.5
Al	1.4		1.0	1.7	2.6
Cu	1.3		1.0	1.6	2.8
Sn	1.7		1.0	2.0	2.8
Pb	1.0		1.0	1.4	1.7
Bi	1.2		1.0	1.6	1.9
U	1.4		1.0	1.7	2.5

IV Analysis

Uniform Density Model

The present experiment gives two bits of data, σ_T and σ_A for each of the nuclei measured. According to the optical model approximation, σ_T is a function of K, the absorption constant; R, the radius; and k_1 the increment in the propagation constant in the nucleus. However, σ_A is a function of K and R only. Noting the definition (4.1) of K we see that σ_A is then a function only of R and $\bar{\sigma}$, the average nucleon-nucleon cross section for bound particles. Therefore, we can deduce R from σ_A by making some assumption on $\bar{\sigma}$ and we have chosen the following:

(a) the average n-n and n-p cross section for bound nucleons is the same as the average n-n and n-p cross section measured at this energy for free nucleons.

The required formulae for the uniform density model as given by Fernbach, Serber, and Taylor (3) are collected in equations (4.1)-(4.4).

$$(4.1) \quad K = \frac{A\bar{\sigma}}{\frac{4}{3}\pi R^3}$$

$$\sigma_A = 2\pi \int_0^R (1 - u^2)\rho\, d\rho$$

in which u is the transmitted amplitude at impact parameter ρ: $u = EXP\left(-K + 2i k_1\right)\sqrt{R^2 - \rho^2}$

$$(4.2) \quad \sigma_A = \pi R^2 \left\{ 1 - \frac{1 - (1 + 2KR)\epsilon^{-2KR}}{2K^2R^2} \right\}$$

$$(4.3) \quad \sigma_T = \sigma_A + \sigma_D = \sigma_A + 2\pi \int_0^R |1-u|^2 \rho\, d\rho$$

$$(4.4) \quad f(\theta) = k \int_0^R (1-u)\, J_0(k\rho \sin\theta)\, \rho\, d\rho$$

To apply these equations, it is convenient to rewrite (4.1) and (4.2) in the form:

$$(4.1\ b) \quad KR = \frac{A\bar{\sigma}}{\frac{4}{3}\pi R^2}$$

$$(4.2\ b) \quad \frac{\sigma_A}{A\bar{\sigma}} = \frac{3}{4KR}\left\{1 - \frac{1-(1+2KR)\epsilon^{-2KR}}{2K^2R^2}\right\}$$

For each value of σ_A the second of these is solved graphically for KR and this value is inserted in (4.1 b) to determine R.   Table 6 collects the absorption and total cross sections measured for Be ... U and the derived values of K and R.   The values of R are also plotted in Figure 16.

The additional information from the measured values of σ_T is used by plotting σ_T/σ_A vs KR (see Figure 17) to compare with the prediction of equation (4.3). It is seen that the measured values are consistent with a single value of $k_1/K = 0.3 \pm 0.1$ for all nuclei.

For the heavy elements, the value of R is essentially equal to $\sqrt{\frac{\sigma_A}{\pi}}$ with only small corrections

Table 6

Summary of Results and Derived Optical Parameters

	Measured Quantities				Derived for $\bar{a} = 43$		Derived for $\bar{a} = 30$	
	σ_A	σ_T	σ_D	σ_T/σ_A	K	R	K	R
Be	187 ±12	308 ±13	121 ±18	1.65 ±13	.41	2.83 ±.21	.15	3.50
C	201 13	378 10	177 16	1.88 .12	.58	2.76 .14	.26	3.20
Al	414 23	703 18	289 29	1.70 .10	.47	3.89 .15	.25	4.26
Cu	674 34	1388 39	714 52	2.06 .12	.60	4.77 .14	.38	4.95
Sn	1158 63	2202 62	1044 88	1.90 .12	.50	6.23 .18	.32	6.40
Pb	1727 45	3209 55	1482 71	1.86 .06	.49	7.55 .11	.33	7.68
Bi	1793 55	3275 62	1482 83	1.83 .07	.47	7.71 .13	.31	7.85
U	1887 98	3640 91	1753 134	1.93 .11	.50	7.89 .22	.33	8.01

All cross sections are in units of 10^{-27} cm.

R is in units of 10^{-13} cm.

K is in units of 10^{13} cm^{-1}.

Least – Squares Fit:

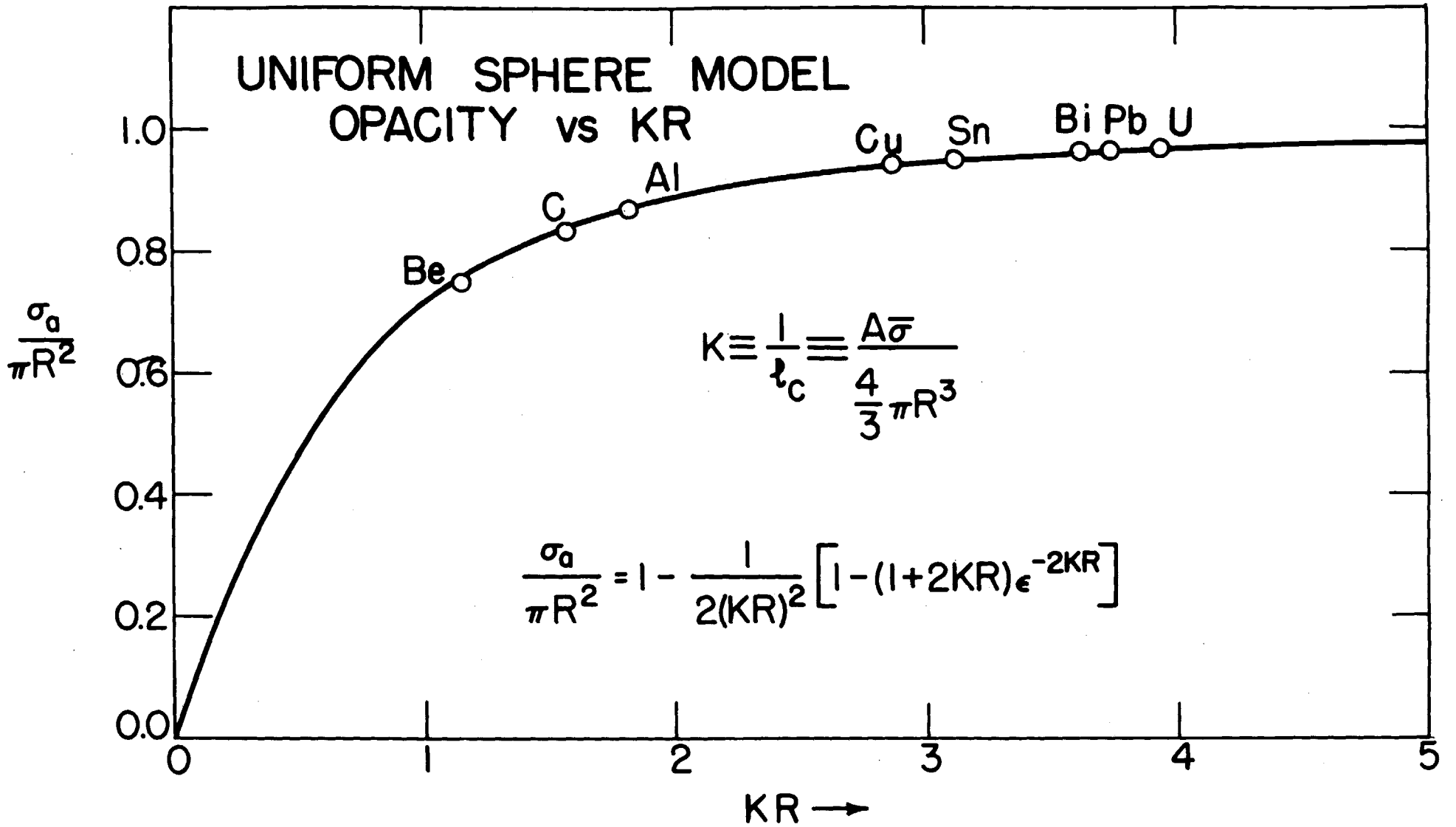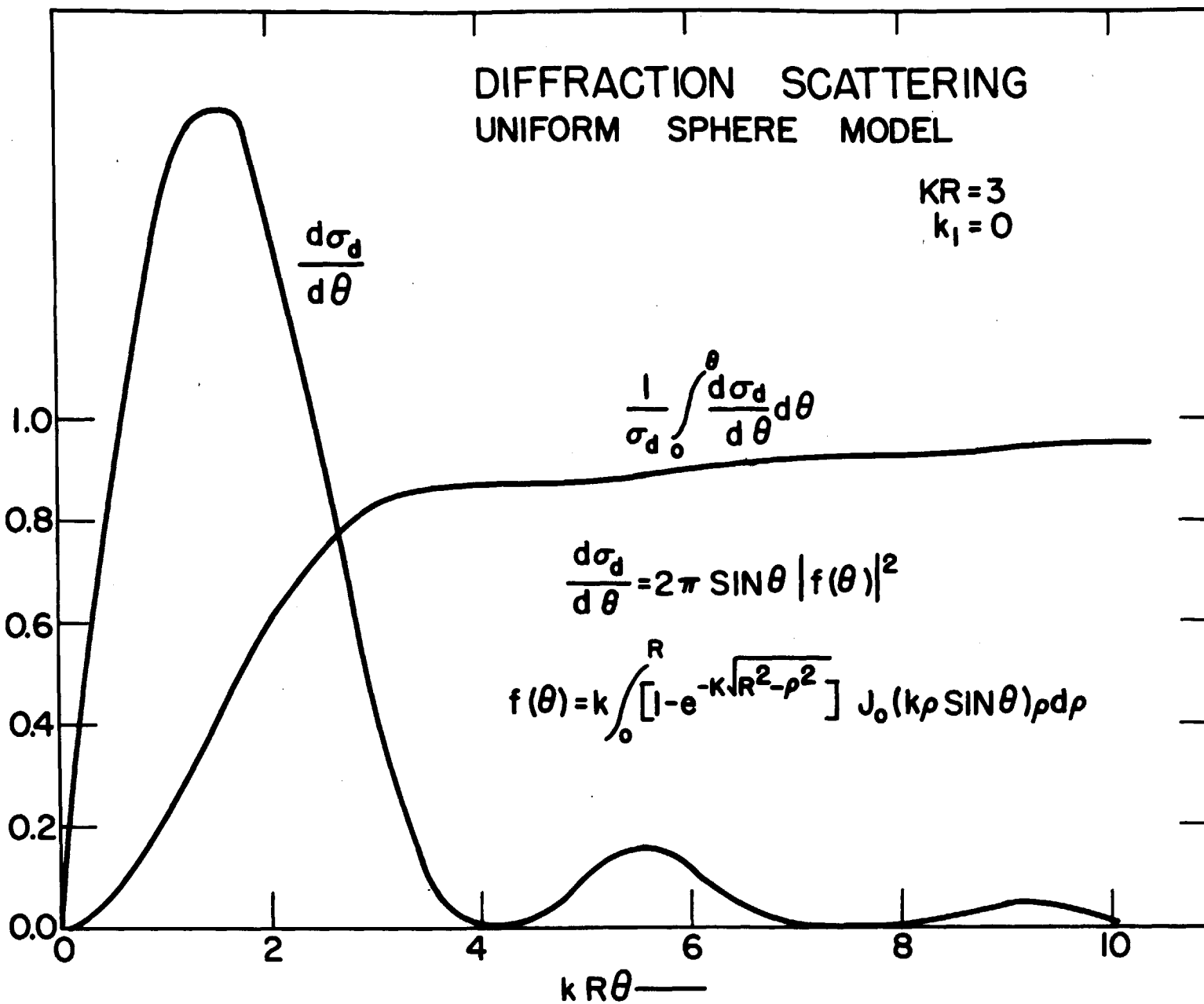$$R = (-0.05 + 1.28\ A^{1/3}) \times 10^{-13}\ cm$$

Figure 16

Figure 17

$\dfrac{\sigma_T}{\sigma_A}$ VERSUS KR FOR UNIFORM DENSITY MODEL

$\dfrac{k_1}{K} = 0.866$

$\dfrac{k_1}{K} = 0.50$

$\dfrac{k_1}{K} = 0.25$

$\dfrac{k_1}{K} = 0$

Cu

Sn

U

Bi

Pb

C

Al

Be

σ_T / σ_A

$KR = \dfrac{A\bar{\sigma}}{\frac{4}{3}\pi R^2}$

UNIFORM SPHERE MODEL
OPACITY vs KR

$$K \equiv \frac{1}{\ell_c} \equiv \frac{A\bar{\sigma}}{\frac{4}{3}\pi R^3}$$

$$\frac{\sigma_a}{\pi R^2} = 1 - \frac{1}{2(KR)^2}\left[1 - (1 + 2KR)\epsilon^{-2KR}\right]$$

Figure 18

DIFFRACTION SCATTERING
UNIFORM SPHERE MODEL

$KR = 3$
$k_l = 0$

$\dfrac{d\sigma_d}{d\theta}$

$\dfrac{1}{\sigma_d}\displaystyle\int_0^\theta \dfrac{d\sigma_d}{d\theta}d\theta$

$\dfrac{d\sigma_d}{d\theta} = 2\pi \, \text{SIN}\,\theta \left| f(\theta) \right|^2$

$f(\theta) = k\displaystyle\int_0^R \left[1 - e^{-K\sqrt{R^2 - \rho^2}} \right] J_0(k\rho\,\text{SIN}\,\theta)\rho\,d\rho$

$k R \theta$ ——
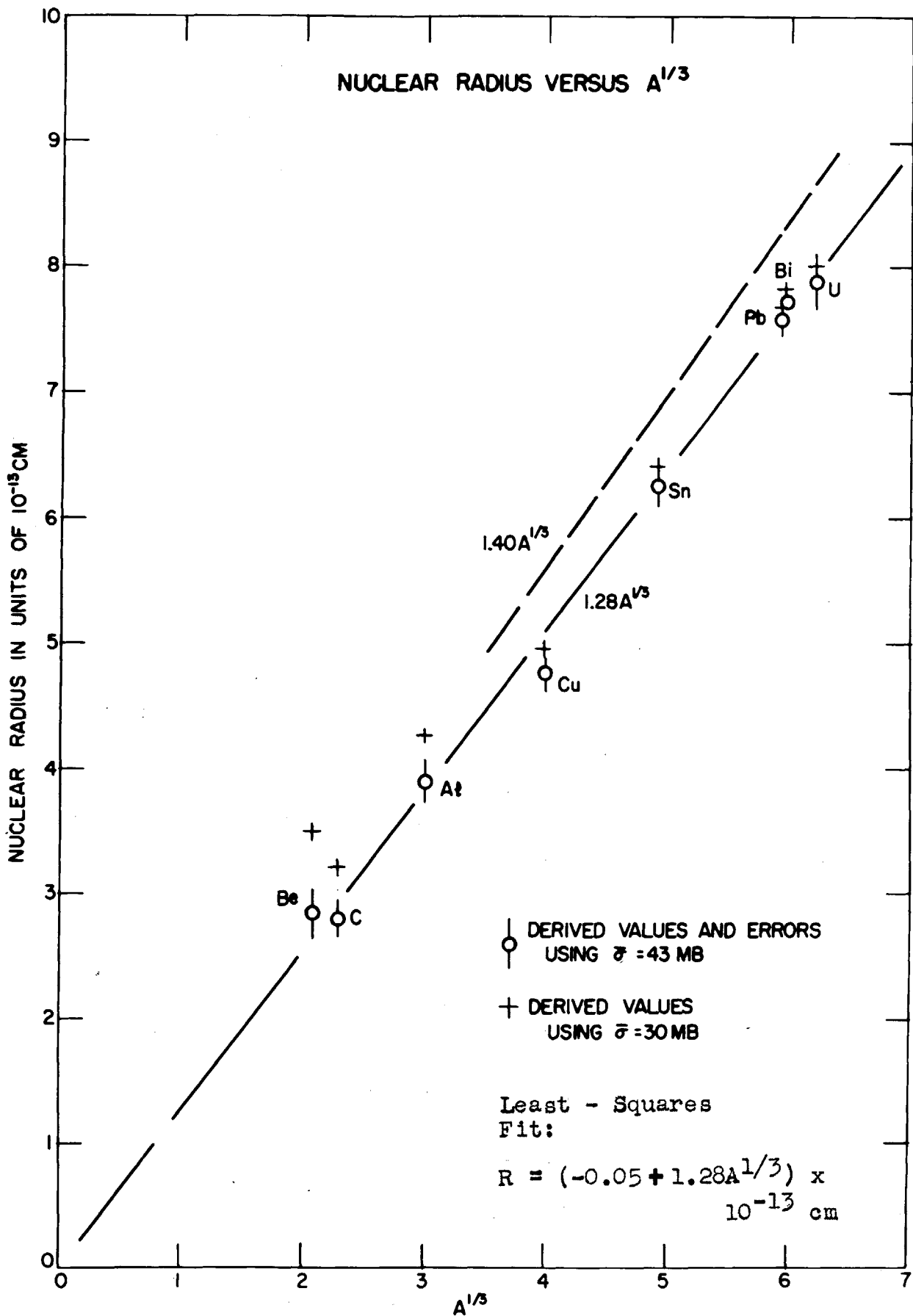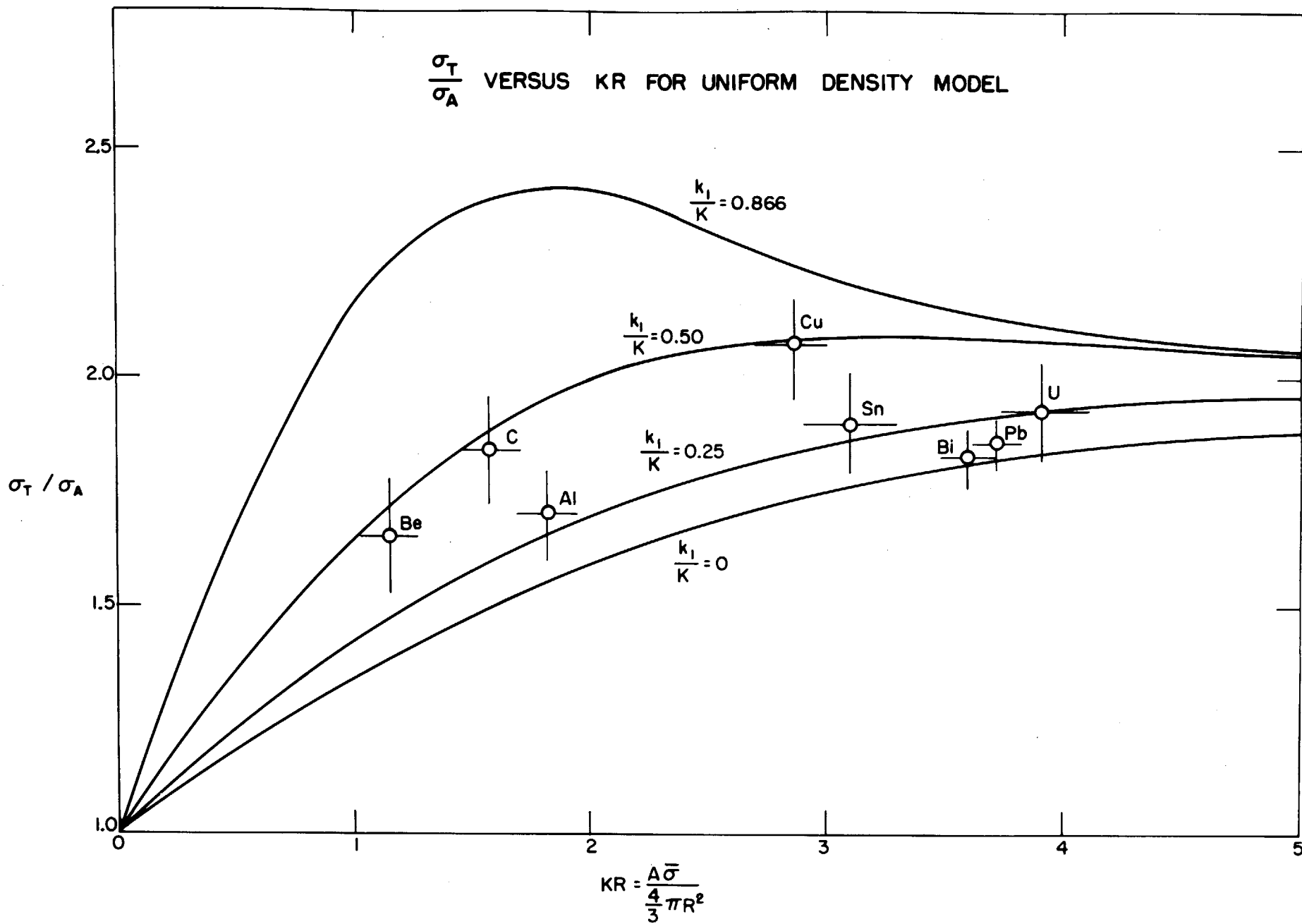
Figure 19

for transparency, hence the derived value of R is rather insensitive to uncertainties in $\overline{\sigma}$. Table 6 and Figure 16 also contain the values of R obtained assuming that $\overline{\sigma}$ = 30 mb.

The opacity function defined by equation (4.2) is plotted in Figure 18; the derived values of $\sigma_A/\pi R^2$ must lie on the curve because the radius is chosen to satisfy (4.2). The angular distribution of equation (4.4) is plotted in Figure 19 for the values $\frac{k_1}{K} = 0$ and KR = 3. For KR this large, the distribution is essentially the diffraction pattern of a black disk.

The interpretation seems consistent in that (1) R is nearly a linear function of $A^{1/3}$, or, in other words, K, which is proportional to nuclear density is reasonably constant except for beryllium and (2) a single value of $\frac{k_1}{K}$ fits the data. The significance of the derived values of k_1, K, and R is discussed in Chapter V.

Gaussian Density

A similar analysis was carried through using the optical model and assuming a gaussian density distribution; this distribution was chosen mainly for ease of calculation although there are arguments based on the shell model which suggest that it may be a realistic one (11). We assume the normalized density of nucleons given by (4.5) and seek to determine the radius parameter, a, for each nucleus.

$$(4.5) \quad P(\imath) = \frac{A}{(a\sqrt{\pi})^3} \epsilon^{-(\imath/a)^2}$$

The path length, t, (in mean free paths) for impact parameter ρ is again gaussian:

$$(4.6) \quad t(\rho) = 2\int_0^\infty P(\sqrt{\rho^2 + s^2})\,\bar{\sigma}\,ds = \frac{A\bar{\sigma}}{\pi a^2}\epsilon^{-(\rho/a)^2}$$

Define: $\quad t_0 = \dfrac{A\bar{\sigma}}{\pi a^2}$

From equation (4.2), σ_A is calculated:

$$(4.7) \quad \sigma_A = 2\pi \int_0^\infty \rho\,d\rho\,(1 - \epsilon^{-t}) = \pi a^2 \int_0^{t_0} \frac{dt}{t}(1 - \epsilon^{-t})$$

$$\sigma_A = \pi a^2 \left\{ \gamma + \ln t_0 - Ei(-t_0) \right\}$$

$$= \pi a^2\,\Omega(t_0)$$

where γ is Euler's constant, $\gamma = 0.5772$, and Ei ($-t_0$) is the exponential integral, Ei ($-t_0$) = $\displaystyle\int_\infty^{t_0} \frac{\epsilon^{-t}}{t}\,dt$
for small t_0 the series expansion (4.8) is useful:

$$(4.8) \quad \sigma_A = \pi a^2 \left\{ t_0 - \frac{t_0^2}{2 \cdot 2!} + \frac{t_0^3}{3 \cdot 3!} - \cdots \right\}$$

for large t_0:

$$(4.9) \quad \sigma_A \simeq \pi a^2 \left[\gamma + \ln t_0 \right]$$

To derive values of the radius parameter, a, from our
data, we rewrite (4.7) in the form:

$$\frac{\sigma_A}{A\bar{\sigma}} = \frac{1}{t_0} \Omega(t_0)$$

solve graphically for t_0, which from the definition (4.6)
gives the value of a. The results calculated on the
assumption that $\bar{\sigma} = 43$ mb are plotted in Figure 20. To
obtain a useful expression for σ_T/σ_A as a function
of t_0, and k_1/K we consider:

$$(4.10) \quad \sigma_T\left(t_0, \frac{k_1}{K}\right) = 2\pi \int_0^\alpha \rho\, d\rho\left\{ (1-w)^2 + 1 - u^2 \right\}$$

$$\sigma_T = 4\pi \int_0^\alpha \rho\, d\rho \left(1 - \epsilon^{-t/2}\right) + 4\pi \int_0^\alpha \rho\, d\rho \left(1 - \cos\frac{k_1 t}{K}\right)\epsilon^{-t/2}$$

where the first integral is $\sigma_T(t_0, 0)$ and is
recognized as:

$$(4.11) \quad \sigma_T(t_0, 0) = 2\pi a^2 \Omega\left(\frac{t_0}{2}\right)$$

The second integral which contains the dependence on k_1/K
is very well approximated for $t_0 > 5$ and $\frac{k_1}{K} > 0.6$ by:

- 40 -

$$4\pi \int_0^{\infty} \rho \, d\rho \, (1 - \cos \frac{k_1 t}{K}) \epsilon^{-t/2} = 2\pi a^2 \int_0^{t_0} \frac{dt}{t} (1 - \cos \frac{k_1 t}{K}) \epsilon^{-t/2}$$

$$(4.12) \qquad \simeq \pi a^2 \left\{ \ln\left[1 + 4\left(\frac{k_1}{K}\right)^2\right] + 2 \, Ei\left(-\frac{t_0}{2}\right) \right\}$$

And for $\frac{k_1}{K} t_0 \ll 1$:

$$\simeq 4\pi a^2 \left(\frac{k_1}{K}\right)^2 \left\{ 1 - (1 + \frac{t_0}{2}) \epsilon^{-t_0/2} \right\}$$

Using these results, σ_T / σ_A is plotted as a function of t_0 for $\frac{k_1}{K} = 0, 0.6, 1.0$ in Figure 21.

RADIUS PARAMETER, a, VERSUS $A^{1/3}$
GAUSSIAN DENSITY MODEL
$\rho = \rho_0\, e^{-(r/a)^2}$

RADIUS PARAMETER, a, IN UNITS OF 10^{-13}CM

Bi
U
Pb
Sn

$a = 0.3 + 0.63\, A^{1/3}$

Cu

Al

Be
C

Least − Squares Fit:
$a = (0.32 + 0.62\, A^{1/3} \times 10^{-13}$ cm

$A^{1/3}$

Figure 20

$\dfrac{\sigma_T}{\sigma_A}$ VERSUS t_0 FOR GAUSSIAN DENSITY MODEL
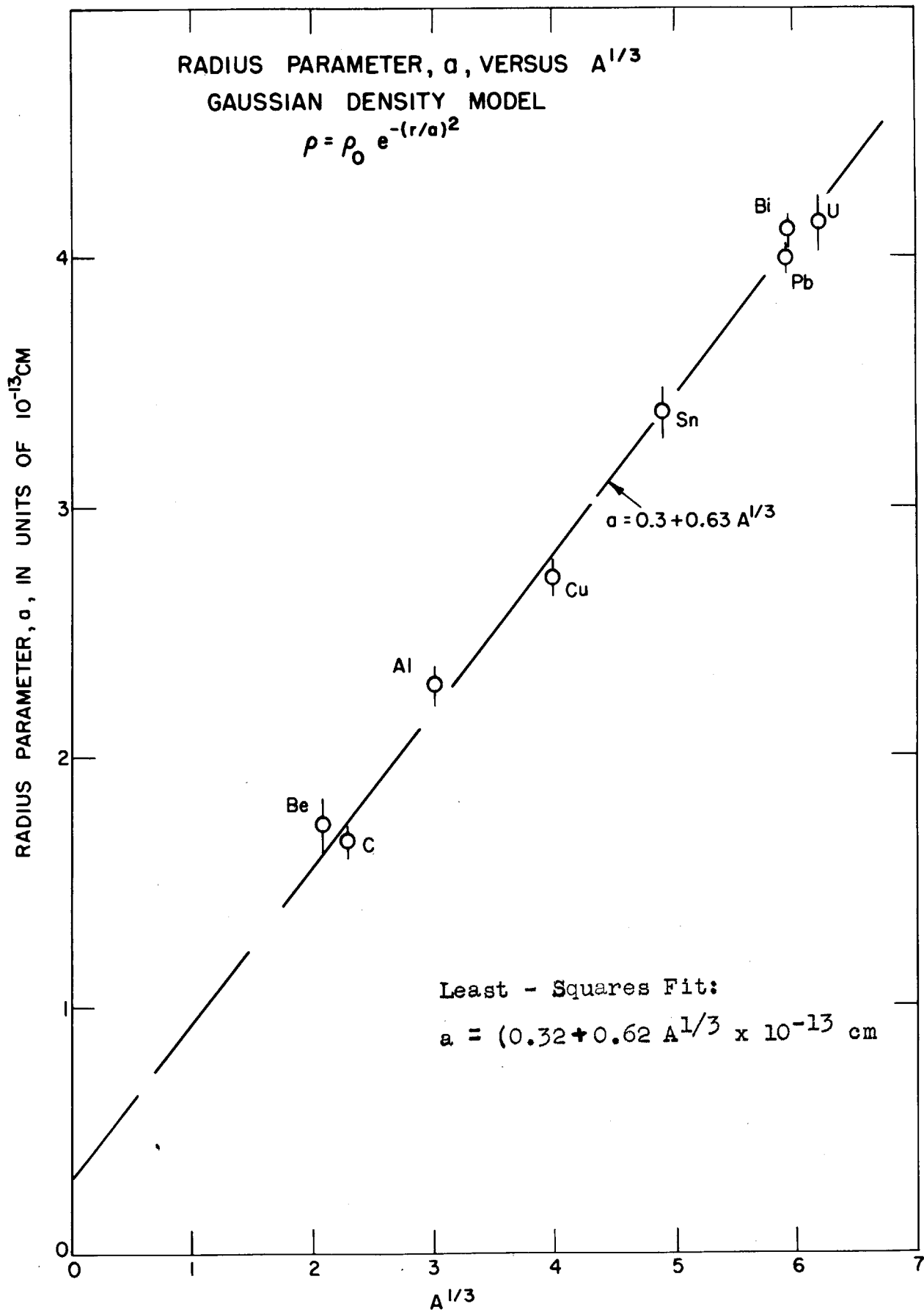
Figure 21
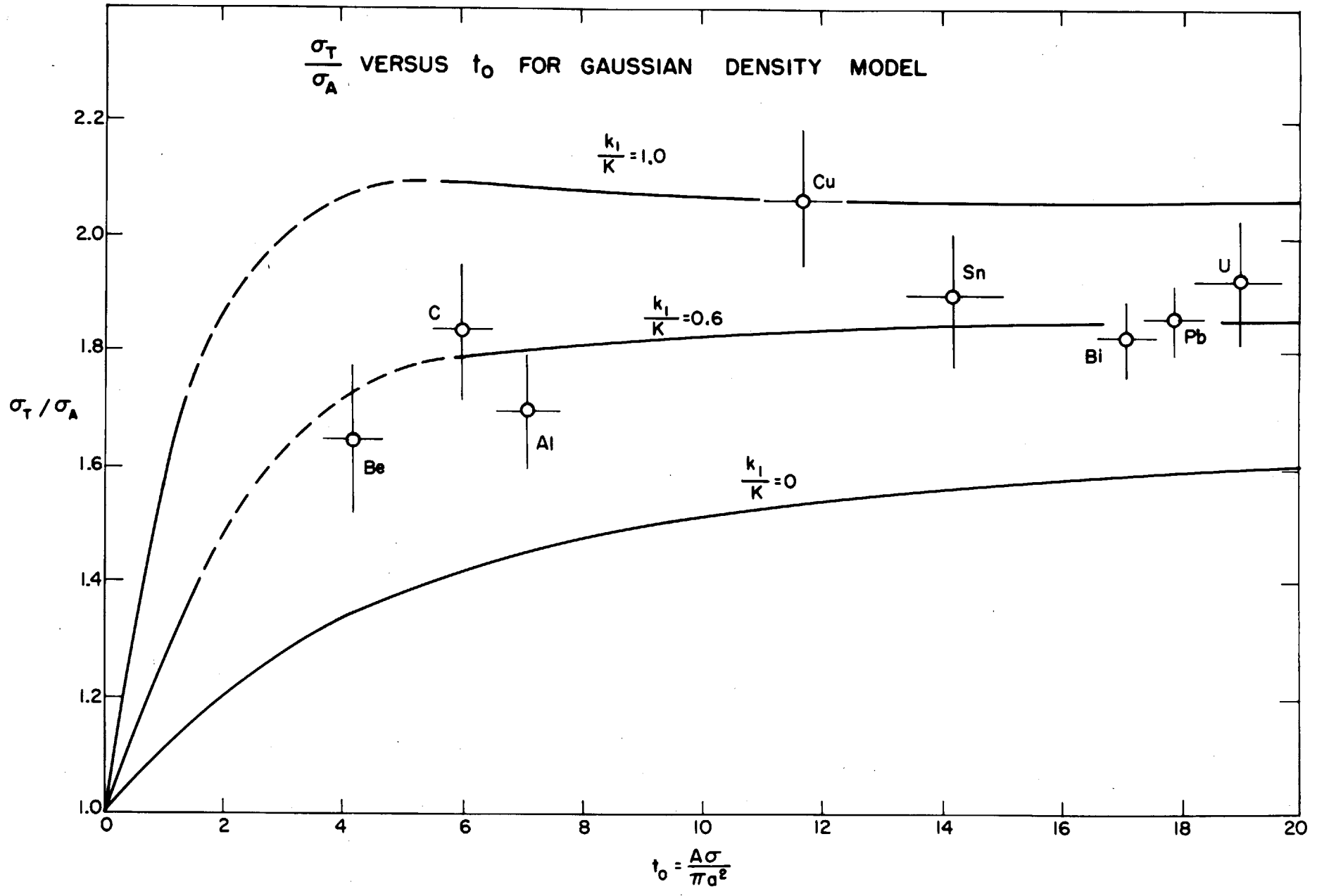
V Interpretation and Conclusions

Effect of Neutron Energy Spectrum and Assignment of Mean Effective Energy

The fact that a broad energy spectrum must be employed in this experiment probably is not as serious an objection to the method as it might appear at first sight. The expectation is that the cross sections of interest are not strongly energy dependent in the energy range from about 1 to 2.2 Bev. In fact, if the nuclear cross sections were a linear function of energy there would be only a slight error in our assignment of the measured cross sections to the mean effective energy of 1.4 Bev. The measured cross section is, of course, an average over the effective energy spectrum given by:

$$(5.1) \quad \sigma_{EXP} = \frac{\int \sigma(E) \, n(E) \, \epsilon(E) \, dE}{\int n(E) \, \epsilon(E) \, dE}$$

(thin scatterer approximation)

in which n(E) is the energy spectrum of the neutron beam, and e(E) is the energy dependence of the detection efficiency.

If we assume that:

(a) the cross section in the energy range considered is a linear function of energy, that is:

$$\sigma(E) = \sigma(\bar{E}) + \sigma'(\bar{E}) \times (E - \bar{E})$$

(b) the mean effective neutron energy defined by the
diffraction scattering angular distribution (as described
in Chapter III) is approximately a linear average in
energy, that is:

$$\bar{E} \simeq \frac{\int E n \epsilon \, dE}{\int n \epsilon \, dE}$$

This second assumption is made reasonable by the calculation
shown in Figure 18. Then the equation (5.1) can be
rewritten:

$$(5.2) \quad \sigma_{EXP} \simeq \sigma(\bar{E}) + \sigma'(\bar{E}) \frac{\int (E - \bar{E}) n \epsilon \, dE}{\int n \epsilon \, dE}$$

but $\int (E - \bar{E}) n \epsilon \, dE = 0$ in virtue of (b).
Therefore $\sigma_{EXP} \simeq \sigma(\bar{E})$ that is, the measured
cross section should be assigned to the mean energy $\bar{E}$. The
correction term can depend only on some average value of $\frac{d^2\sigma}{dE^2}$
over the effective energy spectrum.

To determine whether the estimate of mean energy
depends critically on the nuclear model, a numerical cal-
culation was made of the angular distribution expected for
a gaussian density model. The optical approximation of
equation 4.4 was used, taking radius parameter for lead,
a = 4.0 x 10^{-13} cm, derived in Chapter IV and, assuming
for simplicity that k_1 = 0. (Calculations by Sternheimer (12)
on the uniform model indicate that the principal effect of
making $\frac{k_1}{K}$ = 0 is on the magnitude of the scattering cross

section, the angular distribution is only slightly modified for small values of $\frac{k_\perp}{K}$.) The gaussian model calculation for lead (taking $k_\perp = 0$) yields an angular distribution almost indistinguishable from the uniform model calculation for the first lobe of the diffraction pattern. The second lobe is present but reduced in size to about one third of the uniform model value. The important point is that the angular half width of the diffraction pattern for lead is practically the same for the uniform and the gaussian density models which are fitted to the same absorption cross section. Therefore, the mean energy estimate of 1.4 $\pm$ 0.2 Bev seems insensitive to the choice of nuclear model.

A study has been made by the Brookhaven cloud chamber group (13) of energetic three-prong events produced in a hydrogen-filled chamber by the forward neutron beam. Of some 150 events observed, about 100 are of the type

$$n + p \rightarrow n + p + \pi^+ + \pi^-$$: the remaining events are

$$n + p \rightarrow p + p + \pi^-$$ and $$n + p \rightarrow p + p + \pi^- + \pi^0.$$

The mean primary energy for these three types of events is observed to be 1.7 Bev. Whether or not this value is consistent with the value 1.4 Bev from the present experiment is not clear, since neither the energy dependence of the meson production process nor the energy response of the neutron detector is known.

A mean effective energy as low as 1.4 Bev for the forward neutron beam is rather unexpected and seems to imply that the neutrons emerging from inelastic processes remain well collimated in the forward direction. An alternative, of course, is that the cross section for the elastic charge-exchange process at these energies 2.2 Bev has become considerably smaller than the cross section for inelastic processes.

Interpretation of the Deuteron Total Cross Sections

The interpretation of the total n - D cross section in terms of the free n-p and n-n cross sections is a formidable problem; a simple addition of the elementary free cross sections to obtain σ_D may fail because of (1) coherent scattering from the two nucleons causing interference effects (2) effects of the Pauli principle in excluding some final states, and (3) the effect of the momentum distribution of the bound particles. Glucksterne and Bethe, (14) and G. Chew (15) have written several papers on the problem; the first authors interpret the 90 Mev n - D total cross sections by using a static potential model and the Born approximation. They conclude that simple additivity may fail by about 20% even at that energy; furthermore, the (n-D) total cross section may be greater or less than the sum (n-n) plus (n-p), depending on the exchange character assumed for the (n-n) interaction.

Glucksterne and Bethe note that the failure of

additivity is more marked for the elastic n-D cross section which is almost half the total at 90 Mev. They estimate that the elastic part should remain roughly a constant fraction of the total at higher energies.

Relation of Absorption and Total Cross Sections to Previous
    Results

Table 7 is a partial list of inelastic and total cross sections previously reported for six elements, H, D, C, Al, Cu, and Pb for neutron energies of 39 Mev and above; much of this data has been summarized by Rossi (16) and Hildebrand (17). The results of the present experiment are included as are the recent Brookhaven results (18) for protons from 0.41 to 1.275 Bev. The data of Table 7 is displayed in Figures 22, 23, and 24.

It is striking that the hydrogen and deuterium total cross sections are considerably larger at 1.4 Bev than in the 300 Mev region. According to the optical model, the increased value of $\bar{\sigma}$ should be reflected in an increased value of σ_A particularly for the light elements. For example, if $\bar{\sigma}$ increases from 30 mb at 300 Mev to 43 mb at 1.4 Bev, the absorption cross section of carbon should increase by about 12% over this energy range. The increase in the lead absorption cross section should be only 2.5%. Unfortunately the available data is not accurate enough to argue for or against such an increase.

There is a significant increase in the total cross

Table 7 – Total and Absorption Cross Sections for High Energy Neutrons
(cross sections in millibarns)

Mean Energy (Mev)	Reference	H σ_T	D σ_T	C σ_A	C σ_T	Al σ_A	Al σ_T	Cu σ_A	Cu σ_T	Pb σ_A	Pb σ_T
39	Taylor (19)	223 ±8			1100 ±20						
42	Hildebrand (20)	203 ±7	289 ±13		1089 ±11		1782 ±20		2540 ±19		4440 ±50
64.5	Taylor (19)	126 5			784 20						
83	Bratenahl (21)					500 50	1140 30	910 50	2150 40	1850 180	4470 110
85	Cook (1)	83 4	117 5		550 11		1120 20		2220 40		4530 90
95	De Juren (22)	73 15	104 4	222 9	498 3	418 17	993 11	782 13	2000 20	1750 50	4480 30
97	Taylor (19)	73.9 3			508 20						
115	De Juren (23)						733 12		1490 20		3710 60
150	De Juren (23)								1310 40		
156	Taylor (19)	46.4 1.2	70.7 2		330 3		677 11		1376 18		3499 26

Table 7 – Total and Absorption Cross Sections for High Energy Neutrons – continued

(cross sections in millibarns)

Mean Energy (Mev)	Reference	H σ_T	D σ_T	C σ_A	C σ_T	Al σ_A	Al σ_T	Cu σ_A	Cu σ_T	Pb σ_A	Pb σ_T
160	De Juren (23)	51.2 ±2.6			296 ±6						
180	De Juren (23)						575 ±13		1250 ±30		3060 ±60
190	De Juren (23)				291 9		540 28		1150 40		2850 10
220	De Juren (23)	41 2.4			285 6		576 20		1150 35		2990 140
240	De Juren (23)						576 12		1150 20		2880 50
270	De Juren (24)	38 1.5	57 3	145 6	288 3		555 8	573 24	1145 15	1420 60	2840 30
280	Fox (25)	33 3	49 5		279 4		566 18		1190 20		2890 30
300	Ball (26)			203 33	282	390 23	577	755 33	1170	1720 80	3060
400	Nedzel (27)	33.6			298 3		588 6		1190 10		2890 30
860	Chen (5) (protons)			(222)		(394)		(708)		(1620)	
1400	This Experiment	42.4 1.8	84.6 2.6	201 13	378 10	414 23	703 18	674 34	1388 39	1727 45	3209 55

Figure 22
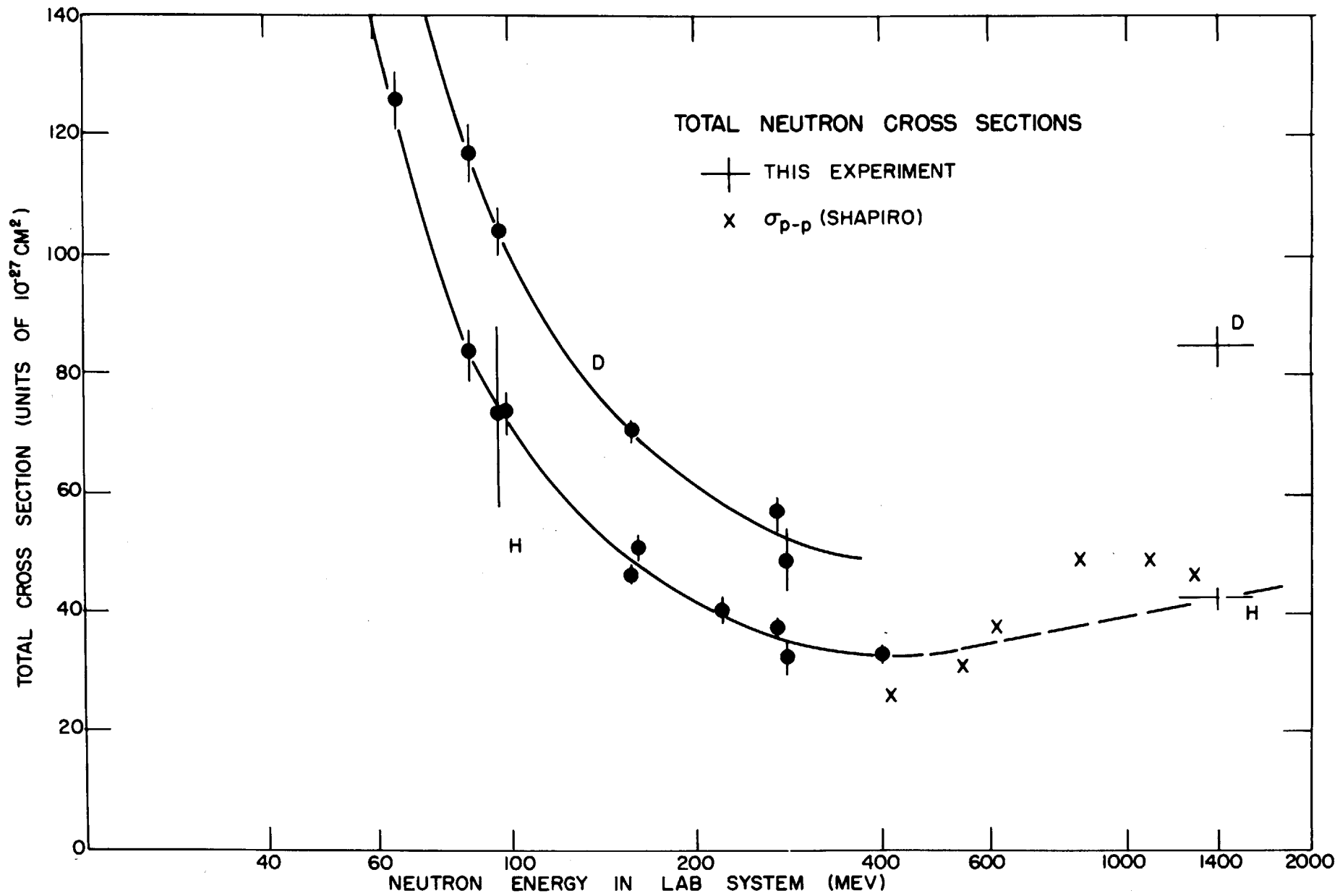
Figure 23
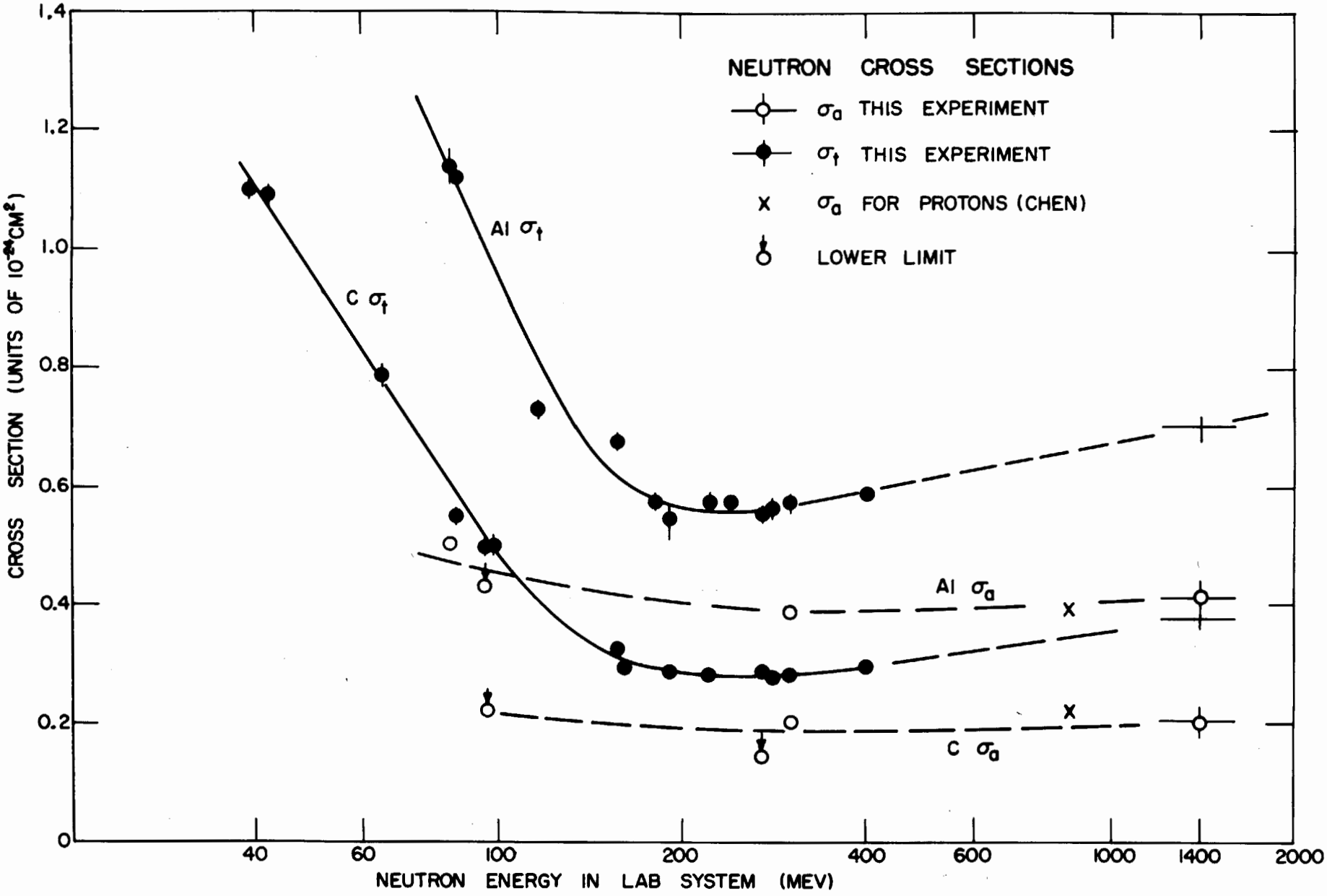
Figure 24
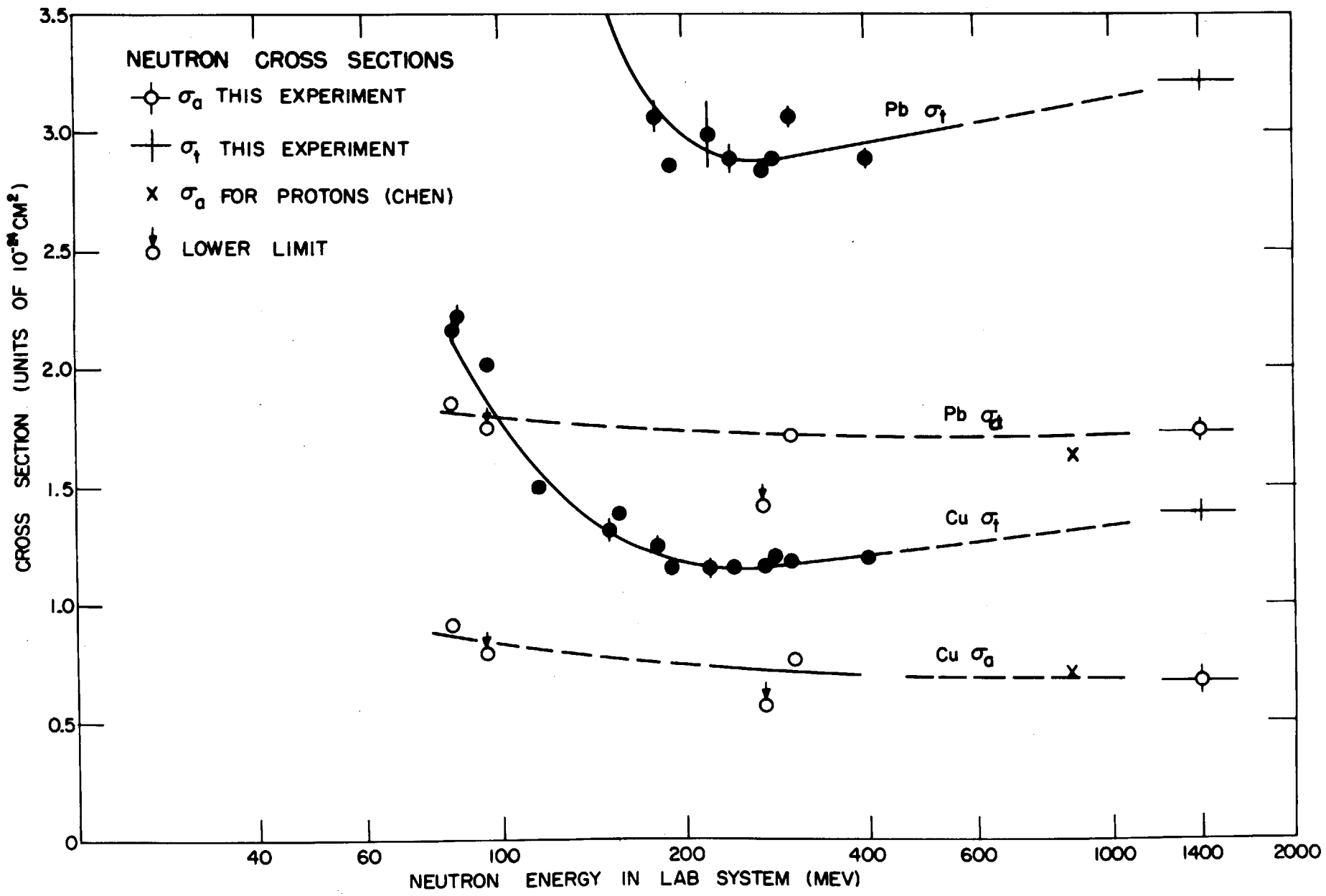
sections of nuclei in the same energy range which probably cannot be explained by the rise in $\bar{\sigma}$ but requires an increase in the optical parameter, k_1.

The Optical Parameters, K and k

The analysis of Chapter IV in terms of the uniform density model leads to the average values of the optical parameters:

(5.3)
$$K = 0.49 \times 10^{13} \text{ cm}^{-1}$$
$$k_1 = (0.15 \pm 0.05) \times 10^{13} \text{ cm}^{-1}$$

Both values are considerably larger than those used to fit the data in the 300 Mev region according to the analysis of Taylor (28). The increase in K reflects the increased nucleon-nucleon cross section. However, we note that the derived value of K is sensitive to the assumptions made about the effective cross section for bound nucleons. For example, if the effective $\bar{\sigma}$ is assumed to be 30 mb instead of 43 mb; the derived value of K is decreased about 35% for the heavy elements but by more than a factor of two for the light elements Be and C.

The gaussian model analysis gives almost the same density at the center for all elements so that only the width varies with A. Assuming $\bar{\sigma}$ = 43 mb and fitting the measured absorption cross sections, this maximum density is required to be about five times that of the uniform model.

The constant k_1 can be related to an average nuclear potential. Taking the relativistic relation (5.4)

and the uniform model value, $k_1 = (0.15 \pm 0.05) \times 10^{13} cm^{-1}$

(5.4) $\quad k_1 = \dfrac{\bar{V}}{Mc^2} \dfrac{Mc}{\hbar} \dfrac{1}{\beta}$ 	 Approximation for

$$\dfrac{k_1}{k} \ll 1$$

we obtained $\bar{V} = 26 \pm 9$ Mev. It is questionable whether an "average nuclear potential" has significance at these energies; however, k_1 is also related to the real part of the average nucleon-nucleon forward scattering amplitude through equation (5.5). (For a derivation of this, see Memmert (29)).

(5.5) $\quad k_1 = \dfrac{2\pi\rho}{k} Re\, f(0)$

(ρ is the density of nucleons)

The value $k_1 = (0.15 \pm .05)\, 10^{13}\, cm^{-1}$ corresponds to Re f (0) $= (2.1 \pm 0.7) \times 10^{-13}$ cm. For the gaussian model, the same calculation gives a value about twice as large.

Nuclear Radii

The data of this experiment can be well fitted with a uniform density model having a radius law of the form $R = b + r_0\, A^{1/3}$, with $b = -.05$ and $r_0 = 1.28$ (in units of $10^{-13} cm$). The previously reported radii as derived from nuclear cross section experiments cannot be well summarized in a short space since the data is quite extensive and the methods of analysis are various.

- 48 -

Cook, et al, give the value $r_0 = 1.37$ from an analysis of the 14 and 25 Mev neutron data; Fernbach, Serber and Taylor (3) find that the 90 Mev neutron data can be consistently fitted with the same value. Taylor (28) has interpreted the 50 to 150 Mev neutron data as well as Nedzel's 400 Mev data to yield values of r_0 from 1.37 for lead to 1.54 for Cu.

Our method of analysis using the absorption cross sections measured by Ball (26) at 300 Mev and assuming $\bar{\sigma} = 27$ mb at that energy, yields $r_0 = 1.31$ for lead and 1.52 for carbon. Gatha and Riddell (30) have used the 340 Mev proton data of Richardson (31) to obtain $r_0 = 1.25$. The recent work of Chen (5) with 860 Mev protons leads to the value $r_0 = 1.25$. The radii deduced from our data are believed to be consistent with most of the previous nuclear scattering experiments, the apparent inconsistencies for the radii of light nuclei are probably not outside the experimental errors.

On the other hand, the recently measured "electro-magnetic" radii are generally about 10 to 20% smaller than the "nuclear force" measurements (32). The μ-mesic X-ray data of Fitch and Rainwater (33) require a uniform model radius r_0 equal to 1.2. The 15.7 Mev electron scattering data of Lyman, Hanson, and Scott (34) are interpreted (35) with a value of r_0 between 1.0 and 1.2. The high energy electron scattering data of Hofstadter, Fechter, and McIntyre (36) seem more consistent with a

non-uniform density model: Schiff (37) has fitted the data
with a gaussian model (although an exponential model is
probably better) and obtains the radius parameter, $a =$
$(3.1 - 3.6) \times 10^{-13}$ cm, as an average for tantalum, gold
and lead. Compare this with the corresponding value
$a = 4.0 \times 10^{-13}$cm., from our data for lead.

Several possible explanations for the smaller
value of the electromagnetic radius have been suggested:

1. The radius measured using a nuclear "probe" should
    naturally exceed the electromagnetic radius by
    approximately the range of nuclear forces.

2. The radius of the proton distribution, which determines
    the electromagnetic radius, is smaller than that of
    the average nucleon distribution.

3. The two sets of radii may be made consistent with a
    proper choice of density distribution. The electro-
    magnetic results depend approximately on the volume
    average, $\langle r^2 \rangle$, while the radii deduced from ab-
    sorption cross sections depend only on the two-
    dimensional "projected" density distribution. For
    example, the uniform-model radius of the lead nucleus
    from the present experiment is about 7% larger than
    the uniform-model radius from the experiment of Fitch
    and Rainwater. However, the gaussian-model radius
    for lead from the present experiment is about 16%
    smaller than the gaussian-model radius given by
    Rainwater (38).

Comparison With Cosmic Ray Results

The cosmic ray data on the absorption of the high-energy nucleon component provides information on the absorption cross sections for nucleons of much higher energy than those used in this experiment. Table 8 collects some of the cosmic ray data for comparison with our results. There seems good evidence that the absorption length decreases with increasing primary energy (16). In particular, λ_A becomes shorter than the value of λ_{GEOM} given by the present data. This result cannot be understood in terms of a uniform-density model but might be explained (43) by a "long-tailed" density distribution if the nucleon-nucleon cross sections increase with energy.

Summary

A counter experiment has been performed at the Brookhaven Cosmotron to measure the absorption and total cross sections of several nuclei for neutrons in the Bev range. The neutrons are produced by bombarding a beryllium target with 2.2 Bev protons. The neutron detector is, in principle, a proton recoil device which requires the incident particle to pass an anti-coincidence counter and produce in an aluminum radiator a charged particle that will penetrate a four-fold scintillation counter telescope containing 6" of lead.

The angular distribution of neutrons measured

Table 8

Comparison with Cosmic Ray Data

1. Present experiment

	Carbon	Lead
λ_A	99 ± 5 gm/cm^2	199 ± 5 gm/cm^2
λ_{geom}	(83 ± 8)	(191 ± 6)

2. Values of λ from cosmic ray data on absorption of N-rays

	Carbon	Lead	Multiplicity of detected event
Walker (39) charged primaries		180 ± 10	N = 4, 5 penetrating 230 gm/cm^2 Pb
		147 ± 10	N > 7 230 gm/cm^2 Pb
Walker, Walker and Greisen (40)			
charged primaries	82 ± 8	157 ± 12	N > 7
neutral primaries	80 ± 7	164 ± 15	230 gm/cm^2 pb
Boehmer and Bridge (41)			
neutral primaries	110	220	
Sitte (42)			
charged primaries		196 ± 13	penetrating 100 gm/cm^2 Pb
		162 ± 10	200 gm/cm^2 Pb

with this detector is sharply peaked forward with a half-width at half-maximum of 6°. The flux of neutrons of energies greater than about 750 Mev is estimated from an emulsion exposure to be 10^3 neutrons per cm^2 per pulse at a distance of 15 meters forward of the target.

Using a narrow collimated neutron beam, the integral angular distribution of diffraction-scattered neutrons from carbon, copper, and lead is determined from attenuation measurements with various detector geometries. The angular half-width of the distribution indicates a mean effective neutron energy of 1.4 ± 0.2 Bev. This method yields approximately a linear average of the neutron energy over the effective spectrum. Although the absolute detector threshold is 0.4 Bev, it is believed that contributions from neutrons below about 1.0 Bev is small.

The total neutron cross sections σ_H and $(\sigma_D - \sigma_H)$ are measured by attenuation differences in good geometry of $CH_2 - C$ and $D_2O - H_2O$ respectively with the results given in Table 2. The cross sections of Be, C, Al, Cu, Sn, Pb, Bi, and U are measured in good and poor geometry; the theoretical angular distribution given by Fernbach, Serber, and Taylor is used to extrapolate the good and poor geometry values to total and absorption cross sections respectively. An important correction to the poor geometry values is made because of the reduced detection efficiency for scattered particles. The total and absorption cross sections from

this experiment are collected in Table 6; a comparison
with previously reported values at lower energy is made in
Table 7 and Figures 22, 23, and 24.

The absorption cross sections are interpreted in
terms of a uniform density nuclear model using an effective
cross section of 43 mb. for bound nucleons. The derived
radii as listed in Table 6 are well represented by
$R = (-.05 + 1.28\ A^{1/3}) \times 10^{-13}$cm. The uniform model analysis
yields the optical parameters, $K = 0.49 \times 10^{-13}$ cm^{-1} and
$k_1 = (0.15 \pm .05) \times 10^{-13}$ cm^{-1}.

The results can be as consistently fitted with a
gaussian-density nuclear model, i.e. $\rho = \rho_0\, \epsilon^{-(R/a)^2}$.
The radius parameter is derived to be $a = (0.32 + 0.62\ A^{1/3})$
$\times 10^{-13}$ cm.

Appendix A

To verify that equation 3.3 takes account of multiple diffraction scattering, consider a typical n-th term which is of the form: $P(n, t) F_n'(\theta)$.

$P(n, t)$ is the probability that <u>only</u> n-fold scattering takes place in thickness t (measured in mean free paths for scattering) and $F_n(\theta)$ is the probability that an n-fold-scattered particle remains in a cone of half angle θ. Assuming that the scattering angles are small so that differences in path length can be neglected, $P(n, t)$ must satisfy the recursion relation:

$$(A-1) \quad P(n, t) = \int_0^t P(1, x) P(n-1, t-x) \, dx$$

since $P(1, x)$ is the probability that only single scattering occurs in thickness x, and $P(n-1, t-x)$ is the probability that only n-1 fold scattering occurs in the remainder t-x. $P(n, t)$ also must have the initial value:

$$(A-2) \quad P(0, t) = \epsilon^{-t}$$

It is seen by substitution that the Poisson distribution (A-3) satisfies conditions (A-1) and (A-2).

$$(A-3) \quad P(n, t) = \frac{1}{n!} t^n \epsilon^{-t}$$

The general problem of finding the angular distribution of n-fold scattering is a difficult one, however, we can achieve a useful result under the

approximations that (a) small angle scattering pre-
dominates and (b) the differential angular distribution of
single scattering is gaussian. Consider first the compounding
of two gaussian distributions of different widths

$$q_a = \frac{d\sigma}{d\omega} \sim \epsilon^{-\frac{\theta^2}{a^2}} \quad \text{and} \quad q_b \sim \epsilon^{-\frac{\theta^2}{b^2}}$$

Figure A-1 depicts the scattering in a plane perpendicular
to the incident particle. The first scattering into the
solid angle $d\omega_1$ at θ occurs with relative probability
$\epsilon^{-\theta^2/a^2}$; the second scattering from $d\omega_1$
at θ to $d\omega_2$ at ξ occurs with probability $\epsilon^{-\varphi^2/b^2}$
with φ, θ, ξ related by equation A-4.
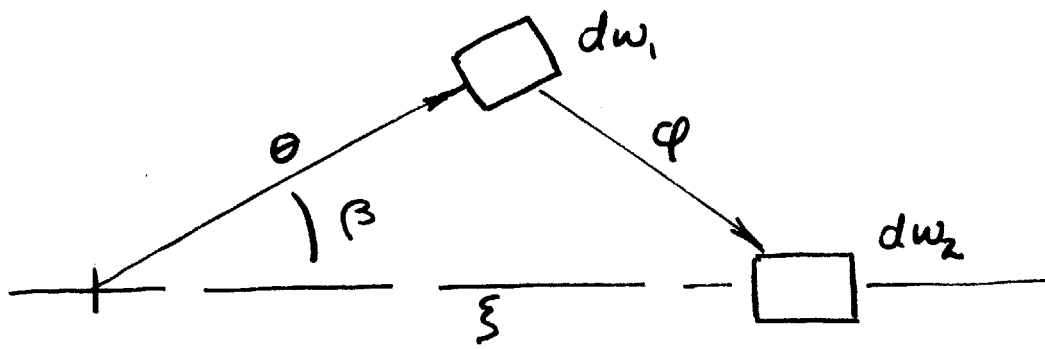
Figure A-1

$$(A\text{-}4) \quad \varphi^2 = \theta^2 + \xi^2 - 2\theta\xi \cos\beta$$

Appendix A

- 2 -

Neglecting constant factors, the probability of compound scattering into $d\omega_2$ at ξ is given by:

$$(A-5) \qquad q_{a+b}(\xi) \sim \iint q_a(\Theta)\, q_b(\varphi)\, d\omega_1$$

$$q_{a+b}(\xi) \sim \int_0^\alpha \int_0^{2\pi} e^{-\Theta^2/a^2}\, e^{-\frac{\Theta^2 + \xi^2 - 2\Theta\xi\cos\beta}{b^2}}\, \Theta\, d\Theta\, d\beta$$

Integration over β yields a zero order Bessel function (of imaginary argument).

$$q_{a+b} \sim \int_0^\alpha e^{-\xi^2/b^2}\, e^{-\Theta^2\left(\frac{1}{a^2}+\frac{1}{b^2}\right)} J_0\left(-\frac{2i\xi\Theta}{b^2}\right) \Theta\, d\Theta$$

The second integration can be expressed in closed form:

$$q_{a+b}(\xi) \sim e^{-\frac{\xi^2}{a^2+b^2}}$$

With this simple rule for compounding, we take $a = b$ and iterate the process n times to get the differential angular distribution of n-fold scattering:

$$q_n \sim e^{-\frac{\xi^2}{n a^2}} \sim q_1\left(\frac{\xi}{\sqrt{n}}\right)$$

Appendix A

- 3 -

Therefore, the fraction of n-fold scattered particles remaining in a cone of half angle Θ is related to the same fraction for single scattering by:

$$F'_n(\Theta) = F'_1\left(\frac{\Theta}{\sqrt{n}}\right)$$

This result, of course, depends essentially on the assumption (b), i.e. a gaussian distribution; and is not valid for more general distributions.

Appendix A

- 4 -

Appendix B

Directionality Correction

The correction for the variation of detection efficiency with angle is calculated from the idealized model of the detector shown in Figure 25. Consider a uniform parallel beam of circular cross section (radius P) incident on a thin scatterer.

A typical particle incident on the scatterer at A (a distance ρ from the axis) is scattered through the space angle θ (and azimuthal angle β) and strikes the radiator at B giving rise to a distribution of charged secondaries in the forward direction with axial symmetry about the line AB. The probability that one of these shall discharge the last counter then depends only on the angle φ between AB and BC where C is the center of the last counter. Summing the contributions to the observed counting rate from all elements of the beam cross section and all scattering angles up to leads to the expression:

$$(B-1) \quad C_{IN}(\xi) = n_0 e^{-t/\lambda_T} \frac{2}{P^2} \int_0^P \rho \, d\rho \, g\left(\frac{\rho}{m}\right) + n_0 S \frac{2}{P^2} \int_0^P \rho \, d\rho \int_0^\xi \psi \, g\overline{(\varphi)} \, d\theta$$

$$(B-2) \quad C_{OUT} = n_0 \frac{2}{P^2} \int_0^P \rho \, d\rho \, g\left(\frac{\rho}{m}\right)$$

$C_{IN}(\xi)$ = Counting rate with scatterer in and detector subtending nominal half angle ξ .

$\xi = \pi/\rho$ for small angles.

C_{oUT} =   counting rate with scatterer out.

$q(\varphi)$ =   probability of detection of neutron

entering radiator at some point B

at angle φ to the line BC.

n_o =   flux of neutrons incident on scatterer

S =   probability that a neutron is scattered

and emerges from the scatterer

normalized angular distribution of

scattered particles. i.e.

$$\int_0^\pi \psi(\theta) \, d\theta = 1$$

For small angles:

$$(B-3) \quad \varphi^2 = \left(1 + \frac{1}{m}\right)^2 \theta^2 + \left(\frac{\rho}{m}\right)^2 + 2\frac{\rho}{m}\left(1 + \frac{1}{m}\right)\theta \cos\beta$$

and $\bar{q}$ = average of q over all values of β. In short,

equation (B-1) represents an average of the efficiency q

over (a) the angular distribution ψ, (b) the azimuth

angle β and (c) the cross section of the incident beam.

It is expected to be valid only in the poor geometry

limit since it contains the assumption that essentially

all of the scattered particles strike the radiator. Only

in this limit, is it proper to average q over all values

of β and use the nominal angle ξ for the upper limit

of the average (a) over the angular distribution. To

be exact, this upper limit depends also on ρ and β

but has a mean value of ξ and in the poor geometry limit

Appendix B

- 2 -

the average (a) is insensitive to the upper limit.

The observed transmission T can now be written as:

$$(B\text{-}4) \quad T(\xi) = \frac{C_{IN}}{C_{OUT}} = e^{-t/\lambda_T} + \frac{S\int \rho \, d\rho \int \psi \, \bar{q} \, d\theta}{\int \rho \, d\rho \, q}$$

The function q is expanded in even powers of φ according to equation (B-5), then by using relation (B-3) the average over β is easily taken.

$$(B\text{-}5) \quad q(\varphi) = q_0 \left(1 - a\varphi^2 + b\varphi^2 \dots \right)$$

After the integration over ρ and rearrangement (noting that $T(0) = e^{-t/\lambda_T}$) Equation (B-4) becomes:

$$S\int_0^\xi \psi \, d\theta = [T(\xi) - T(0)] \left\{ 1 - \frac{\left(1 + \frac{R}{m\xi}\right)^2 \left[a - 2b\left(\frac{P}{m}\right)^2\right]\langle \theta^2 \rangle_\xi - b\left(1 + \frac{R}{m\xi}\right)^4 \langle \theta^4 \rangle_\xi}{1 - \frac{a}{2}\left(\frac{P}{m}\right)^2 + \frac{b}{3}\left(\frac{P}{m}\right)^4} \right\}^{-1}$$

$$= [T(\xi) - T(0)] \times C_1$$

In which:

$$\langle \theta^2 \rangle_\xi = \frac{\int_0^\xi \theta^2 \psi \, d\theta}{\int_0^\xi \psi \, d\theta} \qquad ETC.$$

This expresses the "true" integral angular distribution $S\int_0^\xi \psi \, d\theta$ in terms of the observed transmissions $T(\xi) - T(0)$, with a correction factor depending on the moments of the

distribution, the angle ξ , and the constants a, b which enter in the function g. The function g was determined empirically by observing the relative counting rate as the detector is rotated relative to the collimated beam with the radiator remaining fixed in the beam. The result is the angular distribution of penetrating charged secondaries from aluminum as shown in figure 11. The distribution is very well fitted for angles up to 15° by a polynomial of the form (B-5) with the constants:

a = 6.42 × 10⁻³

b = 1.70 × 10⁻⁵   (for φ in degrees)

To evaluate the moments, $\langle \Theta^2 \rangle_\xi$ and $\langle \Theta^4 \rangle_\xi$, which enter the correction term an approximate angular distribution is taken of the form:

$$(\text{B-8a}) \quad \psi_1 = \frac{\Theta}{\eta} \, \epsilon^{-\frac{\Theta^2}{2\eta^2}} \qquad 0 < \Theta < 3\eta$$

$$(\text{B-8b}) \quad \psi_2 = 0.44 \left(\frac{\eta}{\Theta} \right)^2 \qquad \Theta > 3\eta$$

$$(\text{B-8c}) \quad \eta = \frac{(1.5)(57.3)}{\ell R} \qquad (\text{IN DEGREES})$$

For all elements, ψ_1 is a good approximation to the first lobe of the diffraction pattern predicted by the optical model if the angle η at which the maximum occurs, is chosen according to (B-8c). ψ_2 approximates the "tail" of the pattern with the maxima and minima smoothed out; the normalization constant is chosen so that about 87% of the scattering is included in the first lobe. With this choice of ψ_1 and ψ_2 the moments are calculated and inserting these in equation B-7 one obtains the factor C_1, by which the observed value of $T(\xi) - T(0)$ must be multiplied. Figure 26 displays C_1 versus ξ for several values of the parameter kR. The value of C_1 in the good geometry limit, $\xi \to 0$, is gotten by comparing the average efficiency for detecting the scattered particles which are in this case parallel to the axis and uniform over the $2\frac{1}{2}''$ aperture with the efficiency for the unattenuated beam which is parallel and uniform over a $1''$ diameter circle. According to equation B-9, C_1 approaches 1.05 in this limit; note that B-7 gives the same value.

$$(B-9) \qquad \lim_{\xi \to 0} C_1 = \frac{\int_0^P \rho \, d\rho \, g}{\int_0^R \rho \, d\rho \, g} = 1.05$$

However, the correction to the observed transmission vanishes in this limit because $T(\xi) - T(0)$ goes to zero.

Appendix B

- 5 -

It is noted that the effect on the correction of averaging over finite beam size is negligible; that is, if $P \rightarrow 0$ in equation (B-7) the correction is practically unchanged. In other words, the correction in poor geometry is necessary only because of the <u>divergence</u> of the scattered particles which are collected. Had this result been obvious at the outset the derivation would have been much simpler.

When the detector was modified by replacing the third and fourth counters with 4" and 6" diameter counters, the angular distribution, g , was remeasured and found to be about 30% broader than that for the narrow angle telescope. The magnitude of the correction (that is, $C_1 - 1$) was recomputed and is about 30% smaller for the modified telescope.

RADIUS R

RADIUS P

θ

β

B

d

C

LAST COUNTER

ρ

A

BEAM

ℓ

m

SCATTERER

RADIATOR
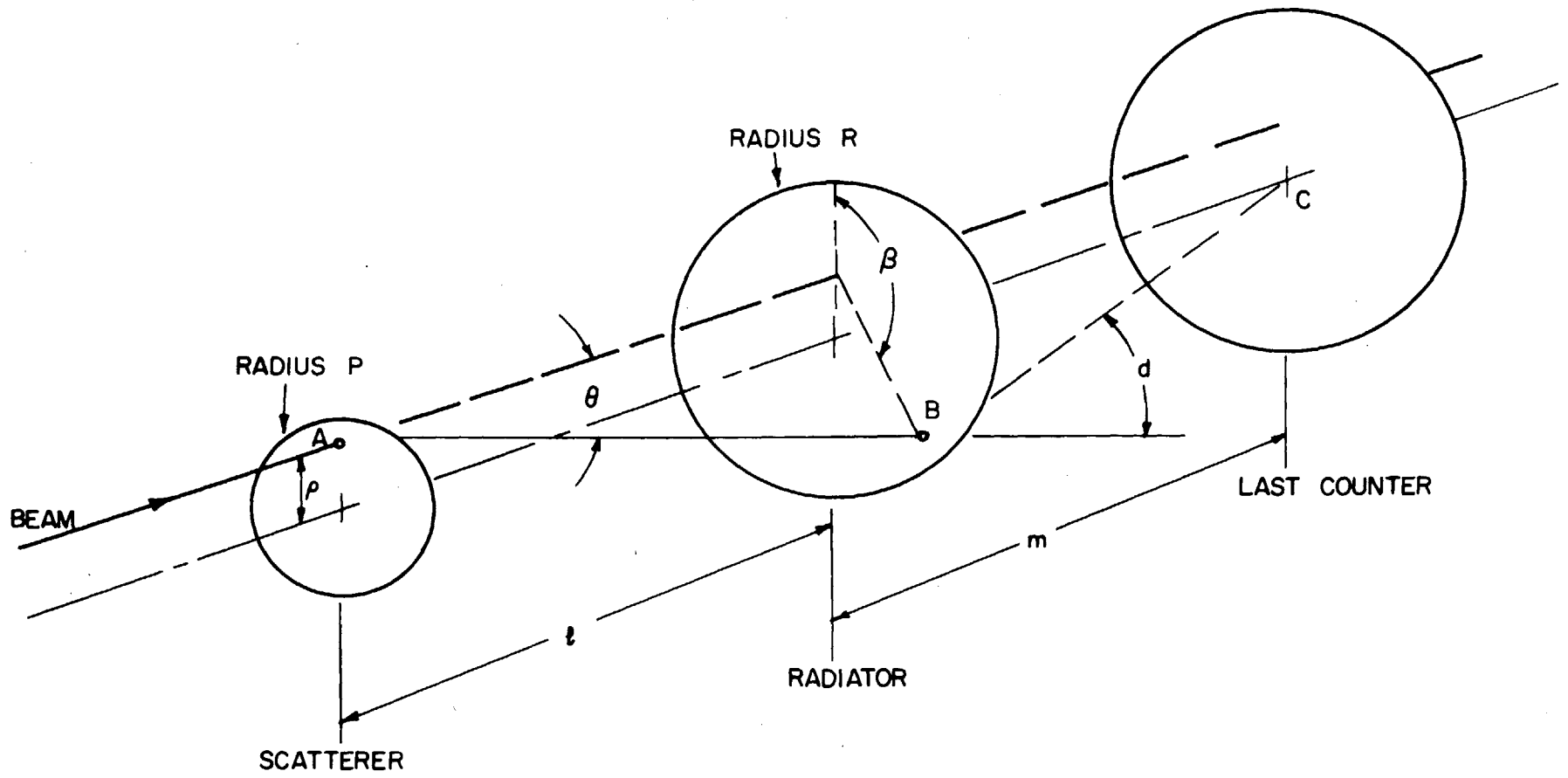
MODEL FOR CALCULATING C_l

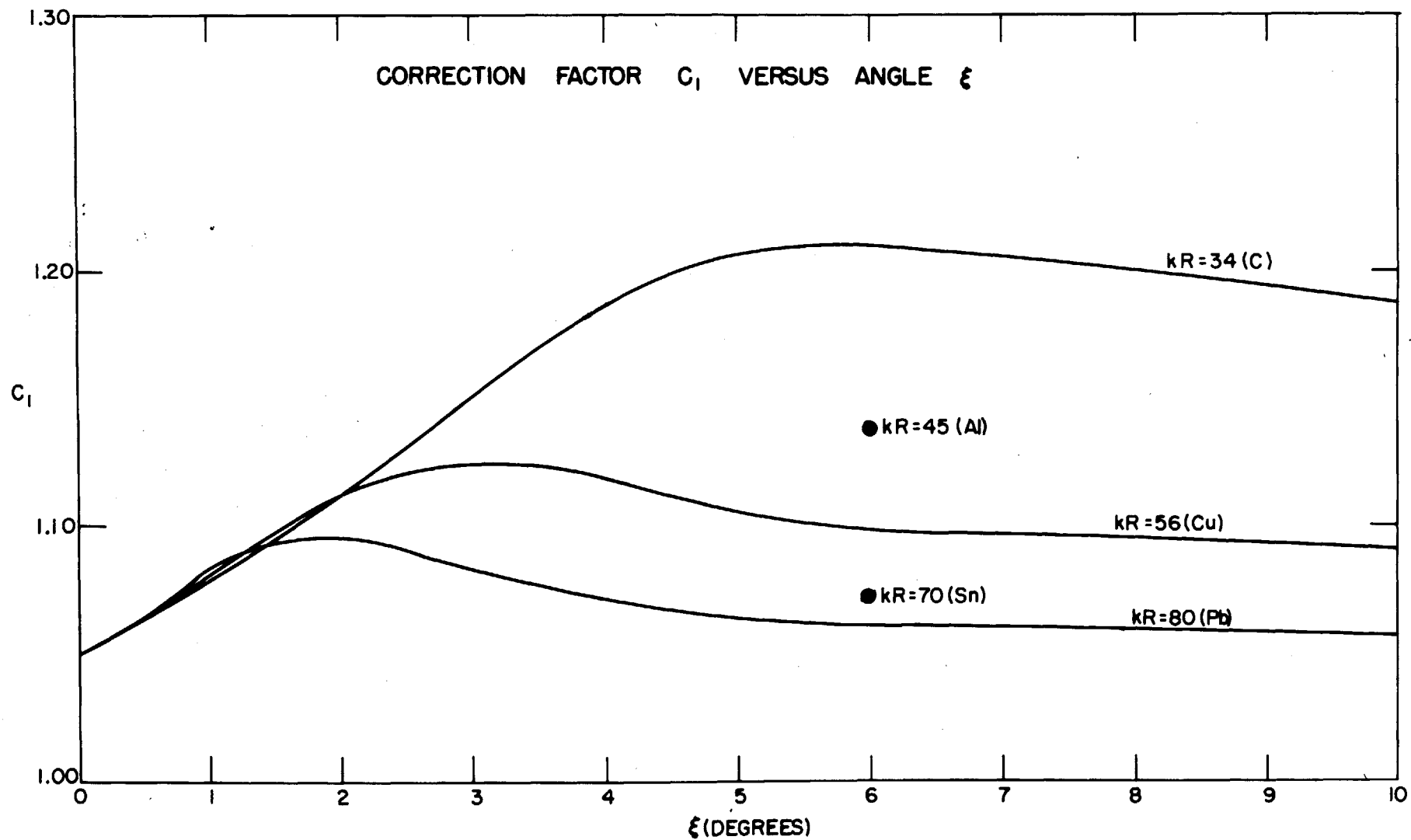Figure 25

CORRECTION FACTOR C_1 VERSUS ANGLE ξ

Figure 26

Appendix C

Finite Beam Size Correction

Because the diameter of the beam (1") is not negligible compared to the aperture of the detector (2½") the angle subtended by the detector is not well defined. To relate the observed transmission to the ideal case of zero beam width a correction is made using the simplified model of figure 27. Consider a uniform parallel beam of circular cross section incident on the scatterer. The probability, h, that a particle scattered at A shall enter the detector is a function of ρ, Θ, R and ℓ. Picturing this scattering in the plane of the detector, it is seen that $h = \dfrac{\beta_1}{\pi}$ in which β_1 is defined as shown by $\dfrac{\ell\Theta}{R}$ and $\dfrac{\rho}{R}$. To make this correction it is assumed that the detection efficiency is uniform and independent of Θ , since these effects were treated indpendently in Appendix B.

Using the notation of Appendix B, the observed counting rates can be expressed as:

$$(C-1) \quad C_{IN}(\xi) = n_0\, e^{-t/\lambda_T} + n_0\, S\frac{z}{P^2} \int_0^P \rho\, d\rho \int_0^\pi \psi(\Theta)\, h\left(\frac{\rho}{R}, \frac{\ell\Theta}{R}\right) d\Theta$$

and $\quad C_{OUT} = n_0$

hence $\quad T(\xi) - T(0) = S\frac{z}{P^2} \int \rho\, d\rho \int \psi(\Theta)\, h\left(\frac{\rho}{R}, \frac{\Theta}{\xi}\right) d\Theta$

Solving the triangle of figure 27, for β_1 we obtain the awkward expression:

$$(C-3) \quad \tan^2\frac{\beta_1}{2} = \frac{\left(1 - \frac{\Theta}{\xi} + \frac{\rho}{R}\right)\left(1 + \frac{\Theta}{\xi} - \frac{\rho}{R}\right)}{\left(1 + \frac{\Theta}{\xi} + \frac{\rho}{R}\right)\left(-1 + \frac{\Theta}{\xi} + \frac{\rho}{R}\right)} \quad ; \quad h = \frac{\beta_1}{\pi}$$

from which h $\left(\frac{\rho}{R}, \frac{\theta}{\xi}\right)$ was calculated for several values of ρ/R. The function h is well approximated by straight line segments according to:

(C-4)

$$h = \frac{1}{2} - \frac{1}{2\pi}\frac{\rho}{R} - \frac{1}{\pi}\frac{R}{\rho}\left(\frac{\theta}{\xi}-1\right) \qquad 1-\frac{\rho}{R} < \frac{\theta}{\xi} < 1 + \frac{\rho}{R}$$

$$h = 0 \qquad \frac{\theta}{\xi} > 1 + \frac{\rho}{R}$$

$$h = 1 \qquad \frac{\theta}{\xi} < 1 - \frac{\rho}{R}$$

The integral in equation (C-2) is then rewritten as

$$S \frac{2}{P^2}\int_0^P \rho\, d\rho \left\{ \int_0^\xi \psi\, d\theta - \underbrace{\int_{\xi-\rho/\!\!\!/}^\xi \psi\, d\theta}_{I} + \underbrace{\int_{\xi-\rho/\!\!\!/}^{\xi+\rho/\!\!\!/} \psi\, h\, d\theta}_{II} \right\}$$

To evaluate I and II, ψ is expanded in Taylor series about ξ, the approximation of (C-4) is used for h and the integration performed. Rearranging (C-2) and using the results of integration we have

$$(C-5) \quad S\int_0^\xi \psi\, d\theta = [T(\xi)-T(0)]\left\{ 1 + \frac{A}{\int_0^\xi \psi\, d\theta} \right\}^{-1} = [T(\xi)-T(0)] \times C_2$$

$$A(\xi) = \sum_{n\ EVEN} \frac{-2}{\pi(m+4)}\left(\frac{P}{R}\right)^{m+2}\frac{\xi^{m+1}\psi^{(m)}}{(m+1)!}$$

$$+ \sum_{n\ ODD}\left\{ -\frac{4(m+1)}{\pi} + 2(m+1) \right\}\left(\frac{P}{R}\right)^{m+1}\frac{\xi^{m+1}\psi^{(m)}}{(m+3)!}$$

$\psi^{(m)}$ = n-th derivative of ψ evaluated at ξ.

This expresses the true integral angular dis-
tribution in terms of the observed value $T(\xi) - T(o)$
and a correction factor C_2 which depends upon ψ and
its derivatives at ξ . Assuming the approximate angular
distributions of Appendix B and inserting the value
$P/R = 0.4$, it is found that the series for A (ξ) converges
rapidly with significant contributions only from terms in
ψ and ψ' . To the extent that the shape of the angular
distribution is the same for each element, the same
correction C_2 applies for each element at corresponding
points in the diffraction pattern. C_2 is plotted as a
function of ξ/n in figure C-2; the scale factor n is
given by $n = (1.5)(57.3)/kR$ degrees according to (B-8c).
The approximate angular distribution of equation (B-8 a, b)
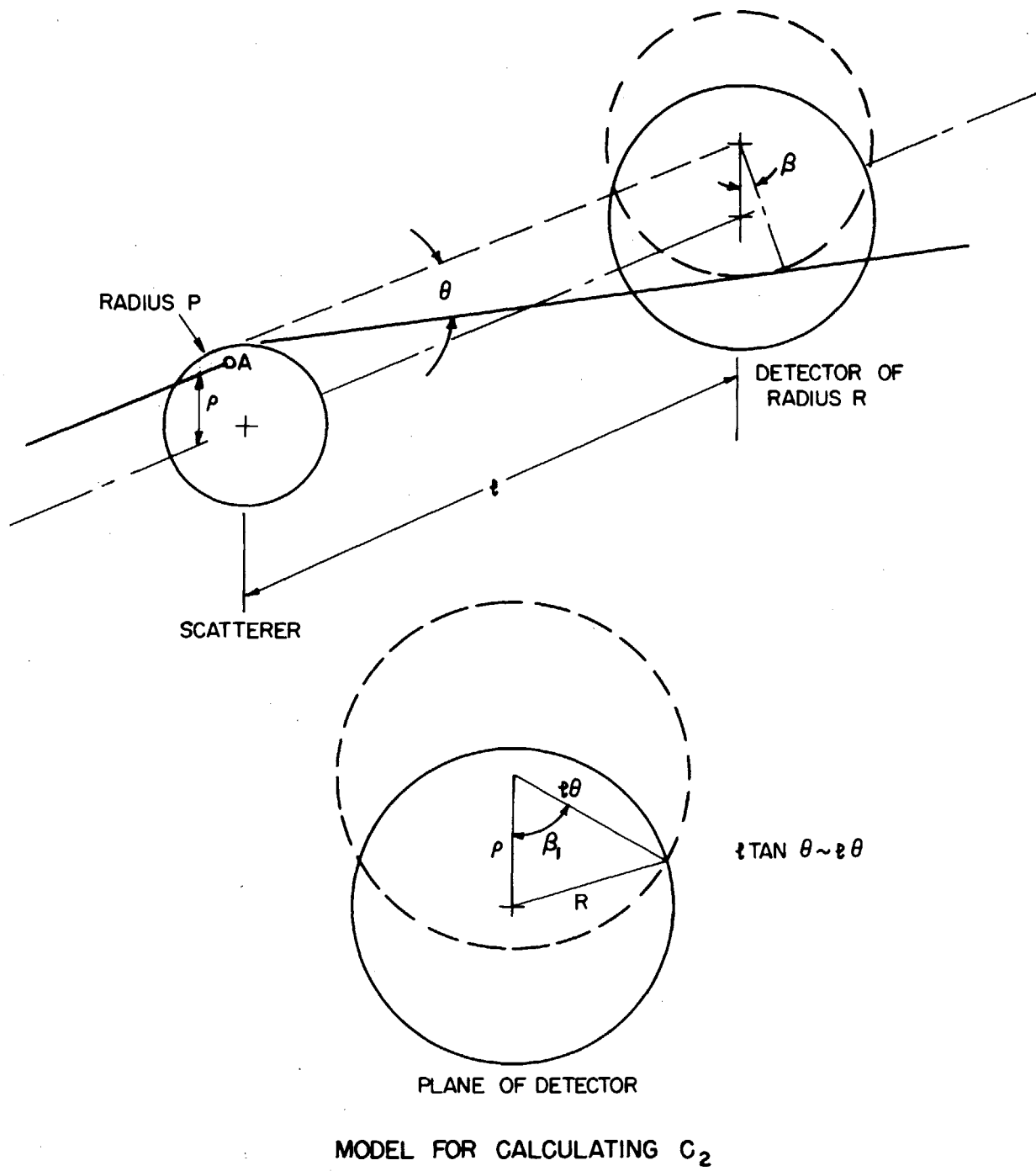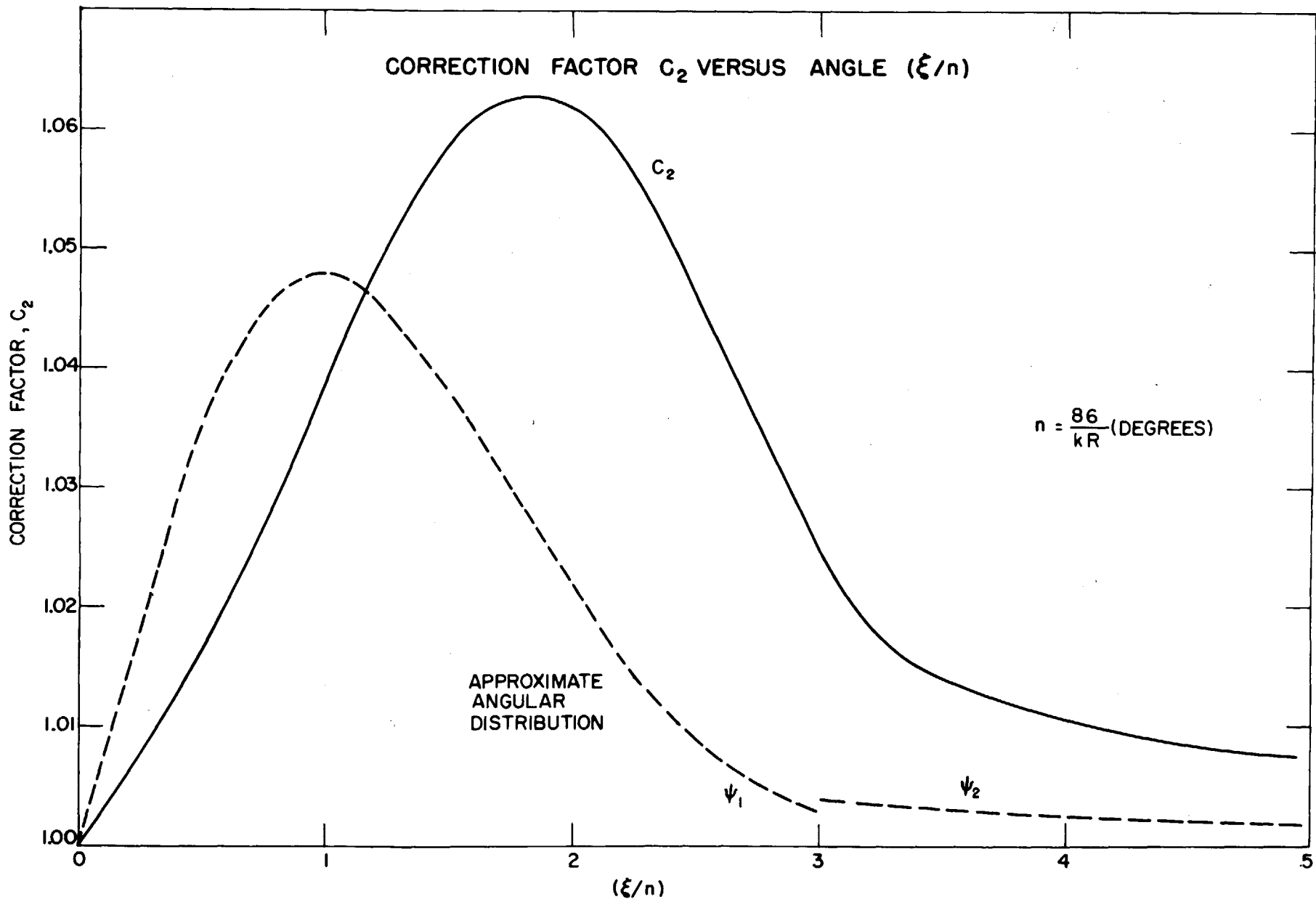is also included in the figure.

RADIUS P

θ

ρ

OA

SCATTERER

β

DETECTOR OF
RADIUS R

ℓ

$\ell\theta$

ρ

β_1

R

ℓ TAN $\theta \sim \ell\theta$

PLANE OF DETECTOR

MODEL FOR CALCULATING C_2

Figure 27

CORRECTION FACTOR C_2 VERSUS ANGLE (ξ/n)

C_2

$n = \dfrac{86}{kR}$ (DEGREES)

APPROXIMATE ANGULAR DISTRIBUTION

ψ_1 ψ_2

CORRECTION FACTOR, C_2

(ξ/n)

Figure 28

References

1 Cook, McMillan, Peterson and Sewell   Phys Rev $\underline{75}$ 7 1949

2 Feshbach and Weisskopf   Phys Rev $\underline{76}$ 1550 1949

3 Fernbach, Serber, and Taylor   Phys Rev $\underline{75}$ 1352 1949
                                                         UCRL 262

4 Pasternack and Snyder   Phys Rev $\underline{80}$ 921 1950

5 Chen, F.   thesis, Harvard University 1954 (unpublished

6 (Cosmotron staff)   Rev Sci Inst $\underline{24}$ 723-870 1953

7 Garwin   Rev Sci Inst $\underline{24}$ 618   1953

8 Widgoff, M. private communication

9 De Juren   UCRL 773

10 Hildebrand   UCRL 1159

11 Born and Yang Proc Phys Soc $\underline{A\ 64}$ 632   1951

12 Sternheimer, R.   private communication

13 Thorndike, A. M.   private communication

14 Glucksterne and Bethe   Phys Rev $\underline{81}$ 761   1951

15 Chew   Phys Rev $\underline{74}$ 809 1948
                                  $\underline{80}$ 196 1950
                                  $\underline{84}$ 710 1951

16 Rossi "High Energy Particles" Prentice-Hall Inc
                                              New York 1952

17 Hildebrand, Hicks and Harker   UCRL 1305

18 Shapiro, Leavitt and Chen Bull Amer Phys Soc $\underline{29}$ No 4 1954

19 Taylor, Pickavance, Cassels and Randle   Phil Mag $\underline{42}$
                                     20, 328, 751 $\underline{1951}$

20 Hildebrand and Leith   Phys Rev $\underline{80}$ 842 1950

21 Bratenahl, Fernbach, Hildebrand, Leith and Moyer   UCRL 431
                                   Phys Rev $\underline{77}$ 597 1950

22 De Juren and Knable Phys Rev $\underline{77}$ 606   1950

References - continued

23   De Juren and Moyer   AECD 2987

24   De Juren   AECD 2854

25   Fox, Leith, Wouters and MacKenzie   AECD 2848
                                    Phys Rev 80 23 1950

26   Ball, W. P.   UCRL 1938

27   Nedzel, U. A. Phys Rev 94 174 1954

28   Taylor, T. B. Phys Rev 92 831 1953 (L)

29   Memmert   Zeit f Physik 134   42 1952

30   Gatha and Riddell   Phys Rev 86 1035 1952

31   Richardson, Ball, Leith, and Moyer Phys Rev 83 859 1951 (L)

32   Cooper and Henley   Phys Rev 92   801   1953

33   Fitch and Rainwater   Phys Rev   92   789   1953

34   Lyman, Hanson, and Scott   Phys Rev 84 626   1951

35   Feshbach and Bitter   Phys Rev 92   837   1953 (L)

36   Hofstadter, Fechter, and McIntyre   Phys Rev 92 978 1953

37   Schiff Phys Rev 92 988   1953

38   Rainwater, quoted in

            Proceedings of the 1954 Rochester Conference
            on High Energy Physics

39   Walker, W. D.   Phys Rev 77   686   1950

40   Walker, Walker, and Greisen   Phys Rev 80 546 1950

41   Boehmer and Bridge, quoted in Rossi (16)

42   Sitte   Phys Rev 78   714   1950

43   Williams, R. W. Bull Amer Phys Soc   29 No. 4 1954

Acknowledgments

Biographical Note

The author was born August 29, 1927 in Syracuse, New York. He spent his childhood there and attended the public schools in that city. Upon graduation from high school, the author entered M.I.T. on a freshman scholarship and completed his first year in November 1945. He then enlisted in the Army, served one year in the U.S. and, obtaining a commission in the Corps of Engineers, served one year in Japan.

The author was admitted to Princeton University in September 1948 and was awarded an A.B. degree, summa cum laude, in June 1951 with election to Phi Beta Kappa, Sigma Xi, and award of the Kusaka Memorial Prize in Physics.

He entered the physics department of the M.I.T. graduate school in September 1951 and held a research assistantship in the Cosmic Ray Laboratory. During the 1952 - 1953 academic year he held a National Science Foundation Predoctoral Fellowship and, in the following year, a research assistantship at the Brookhaven National Laboratory.

The author is married to the former Alice Dean Hanly of Wilmington, Delaware and has a son, Charles Brewster.